Optimum Group Detection for Spatial Multiplexing Systems

by

Byron Paul MAZA CHALAN

THESIS PRESENTED TO ÉCOLE DE TECHNOLOGIE SUPÉRIEURE
IN PARTIAL FULFILLMENT FOR THE DEGREE OF
DOCTOR OF PHILOSOPHY
Ph.D.

MONTREAL, OCTOBER 4, 2023

ÉCOLE DE TECHNOLOGIE SUPÉRIEURE
UNIVERSITÉ DU QUÉBEC

BOARD OF EXAMINERS

THIS THESIS HAS BEEN EVALUATED

BY THE FOLLOWING BOARD OF EXAMINERS

Mr. Georges Kaddoum, Thesis supervisor
Electrical Engineering Department, École de technologie supérieure

Mr. François Gagnon, Thesis Co-Supervisor
Electrical Engineering Department, École de technologie supérieure

Mrs. Bassant Selim, Chair, Board of Examiners
Systems Department, École de technologie supérieure

Mrs. Kuljeet Kaur, Member of the Jury
Electrical Engineering Department, École de technologie supérieure

Mrs. Hanna Abumarshoud, External Independent Examiner
LiFi Research and Development Centre, University of Strathclyde

THIS THESIS WAS PRESENTED AND DEFENDED

IN THE PRESENCE OF A BOARD OF EXAMINERS AND THE PUBLIC

ON SEPTEMBER 15, 2023

AT ÉCOLE DE TECHNOLOGIE SUPÉRIEURE

ACKNOWLEDGEMENTS

I would like to express my gratitude to Prof. François Gagnon and Prof. Georges Kaddoum for the support, guidance, and advice they have provided me in my academic and professional activities.

I would also like to thank the Universidad Técnica Particular de Loja for their support and promotion during my stay as a professor, especially Rommel Torres and Juan Pablo Suárez, for their trust and support.

I want to express my thanks and love to my son Leonel and my wife Verónica for giving me their daily support. Furthermore, I would like to thank my parents, in-laws, brothers, brothers-in-law, and nephews for their support and strong confidence in my academic and personal aptitudes to carry out this doctoral program. I express my gratitude to the Presbyters Sócrates Chinchay and Enry Armijos for their prayers and spiritual support for me and my family.

Finally, I would also like to thank all my friends and colleagues who have closely followed the development of my studies.

"Gratias vobis ago, Señorcito et Churonita! Facite me instrumentum boni."

"*A mis hijos...*"

Détection de groupe optimale pour les systèmes de multiplexage spatial

Byron Paul MAZA CHALAN

RÉSUMÉ

Les grands systèmes MU-MIMO (Multi-User Multiple-Input Multiple-Output) sont des technologies de communication sans fil avancées qui prennent en charge un grand nombre d'antennes aux extrémités de l'émetteur et du récepteur. Ces systèmes assurent le multiplexage spatial, la diversité et la formation de faisceaux, améliorant considérablement la capacité et la fiabilité des communications sans fil. En conséquence, les grands systèmes MU-MIMO sont devenus un composant essentiel des réseaux sans fil 5G et au-delà de la 5G, répondant à la demande croissante de débits de données plus élevés.

Le facteur de charge fait référence au rapport entre le nombre d'équipements utilisateur (UE) et le nombre d'antennes de la station de base (BS). Lorsque le facteur de charge s'approche de zéro, le système atteint des conditions de propagation favorables qui offrent un gain de diversité et une fiabilité significatifs. Dans ce scénario, les récepteurs linéaires tels que le forçage zéro (ZF) et l'erreur quadratique moyenne minimale (MMSE) fonctionnent de manière quasi optimale. En revanche, le système maximise le gain de multiplexage et la capacité lorsque le facteur de charge est égal à un, appelé facteur de pleine charge. Cependant, ce scénario entraîne des conditions de propagation non favorables, dégradant gravement les performances des récepteurs linéaires et en faisant des algorithmes sous-optimaux.

Le récepteur de détection de groupe à vraisemblance maximale (GD-ML) est un algorithme qui améliore les performances des récepteurs linéaires sans augmenter significativement leur complexité. La technique GD-ML consiste à diviser le vecteur de symboles reçus en groupes après application d'une projection linéaire. La détection optimale de vraisemblance maximale (ML) est appliquée à chaque groupe. Bien que cette technique ait été étudiée pour les systèmes conventionnels à entrées multiples et sorties multiples (MIMO) avec canaux Rayleigh non corrélés, son potentiel pour les grands systèmes MU-MIMO reste largement inexploré.

Dans cette thèse, nous visions à atteindre deux objectifs principaux liés à l'efficacité du récepteur GD-ML dans les grands systèmes MU-MIMO avec facteur de pleine charge et canal Rayleigh corrélé. Le premier objectif consiste à obtenir l'équation de la complexité du récepteur et à évaluer le compromis entre performance et complexité. Le deuxième objectif est de dériver une expression analytique des performances du récepteur GD-ML. Les objectifs susmentionnés ont été atteints en utilisant la méthodologie suivante: une revue de la littérature, qui comprenait des travaux pertinents et des informations de base ; création d'un modèle de système qui suppose une infrastructure cellulaire sans fil avec des antennes distribuées et non corrélées de M au niveau de la BS, des UE à antenne unique et corrélés N étroitement situés, et un récepteur GD-ML avec une taille de groupe N_u, ($N \gg N_u$); des métriques d'évaluation qui incluaient le taux d'erreur sur les bits (BER) et le taux d'erreur vectorielle (VER) comme métriques de performances, ainsi que la métrique des opérations à virgule flottante (FLOP) pour la complexité de calcul; analyse mathématique qui impliquait la formulation d'équations analytiques pour évaluer les

performances et la complexité du récepteur à l'aide de la théorie aléatoire multivariée, de l'ordre stochastique et des opérations matricielles.

Nous avons fourni l'équation FLOP pour évaluer la complexité du récepteur GD-ML. Nous avons observé que l'algorithme GD-ML a presque la même complexité que ZF et MMSE, où les étapes de détection ML et de regroupement ajoutent une complexité négligeable à l'opération de projection linéaire. Nous avons dérivé une expression sous forme fermée pour le groupe moyen VER afin d'évaluer les performances du récepteur GD-ML. Nos résultats analytiques ont indiqué que le récepteur GD-ML fournit un gain de diversité proportionnel à $M - N + N_u$. Nous avons également constaté que les performances du récepteur GD-ML diminuent à mesure que les coefficients de corrélation des UE augmentent. Les résultats numériques ont révélé que le récepteur GD-ML surpasse à la fois les récepteurs ZF et MMSE et ont validé l'expression de performance dérivée. Nous avons observé que l'expression analytique et les résultats numériques restent proches pour les petits N_u. À un rapport signal/bruit (SNR) modéré, nous avons observé que les résultats de l'expression analytique et de la simulation correspondent étroitement et deviennent parfaits à mesure que la corrélation des UE augmente.

Mots-clés: détection de groupe, grand MU-MIMO, détection ML, performances VER, canaux corrélés

Optimum Group Detection for Spatial Multiplexing Systems

Byron Paul MAZA CHALAN

ABSTRACT

Large MU-MIMO (Multi-User Multiple-Input Multiple-Output) systems are advanced wireless communication technologies that support a large number of antennas at both the transmitter and receiver ends. These systems provide spatial multiplexing, diversity, and beamforming, significantly enhancing wireless communication's capacity and reliability. As a result, large MU-MIMO systems have become an essential component of 5G and beyond-5G wireless networks, meeting the increasing demands for higher data rates.

The load factor refers to the ratio of the number of user equipment (UEs) to the number of antennas at the base station (BS). When the load factor approaches zero, the system achieves a favorable propagation condition that offers significant diversity gain and reliability. In this scenario, linear receivers such as zero-forcing (ZF) and minimum mean square error (MMSE) perform near-optimal. In contrast, the system maximizes the multiplexing gain and capacity when the load factor equals one, called the full-load factor. However, this scenario results in a non-favorable propagation condition, severely degrading the linear receivers' performance and making them sub-optimal algorithms.

Maximum-likelihood group detection (GD-ML) receiver is an algorithm that improves the performance of linear receivers without significantly increasing their complexity. The GD-ML technique involves dividing the received symbols vector into groups after applying a linear projection. The optimal Maximum-likelihood (ML) detection is applied to each group. While this technique has been researched for conventional multiple-input multiple-output (MIMO) systems with uncorrelated Rayleigh channels, its potential for large MU-MIMO systems remains largely unexplored.

In this thesis, we aimed to achieve two primary objectives related to the effectiveness of the GD-ML receiver in large MU-MIMO systems with full-load factor and correlated Rayleigh channel. The first objective involves obtaining the equation for the receiver's complexity and assessing the compromise between performance and complexity. The second objective is to derive an analytical expression for GD-ML receiver performance. The aforementioned objectives were accomplished using the following methodology: a literature review, which encompassed relevant works and background information; creation of a system model that assumes a wireless cellular infrastructure with M distributed and uncorrelated antennas at the BS, N closely-located single-antenna and correlated UEs, and a GD-ML receiver with group size N_u, ($N \gg N_u$); evaluation metrics that included bit error rate (BER) and vector error rate (VER) as performance metrics, along with the floating-point operations (FLOPs) metric for computational complexity; mathematical analysis which involved the formulation of analytical equations to assess the receiver's performance and complexity using multivariate random theory, stochastic ordering, and matrix operations.

We provided the FLOPs equation to evaluate the GD-ML receiver's complexity. We observed that the GD-ML algorithm has almost the same complexity as ZF and MMSE, where the ML detection and grouping stages add a negligible complexity compared to linear projection operation. We derived a closed-form expression for the average group VER to assess the GD-ML receiver's performance. Our analytical results indicated that the GD-ML receiver provides a diversity gain proportional to $M - N + N_u$. We also found that the GD-ML receiver's performance decreases as the UEs' correlation coefficients increase. Numerical results revealed that the GD-ML receiver outperforms both ZF and MMSE receivers, and validated the derived performance expression. We observed that the analytical expression and numerical outcomes remain close for small N_u. At a moderate signal-to-noise ratio (SNR), we observed that the analytical expression and simulation results closely match and become perfect as the UEs' correlation increases.

Keywords: group detection, large MU-MIMO, ML detection, VER performance, correlated channels

TABLE OF CONTENTS

Page

LIST OF FIGURES

LIST OF ABBREVIATIONS

5G	Fifth-Generation
BC	Broadcast Channel
BER	Bit Error Rate
BEP	Bit Error Probability
BS	Base Station
CDMA	Code-Division Multiple-Access
CPU	Central Processing Unit
CSI	Channel State Information
DoD	Direction of Departure
DoA	Direction of Arrival
EGC	Equal Gain Combining
eMBB	Enhanced Mobile Broadband
eV2X	Enhanced Vehicle-to-Everything
FLOP	Floating-Point Operations
GD-ML	Maximum-Likelihood Group Detection
LAN	Local Area Network
LOS	Line-of-Sight
MAC	Multiple Access Channel
MIMO	Multiple-Input Multiple-Output

MISO	Multiple-Input Single-Output
ML	Maximum-Likelihood
mMTC	Massive Machine-Type Communications
MRC	Maximum Ratio Combining
MRT	Maximum Ratio Transmission
MU-MIMO	Multi-user MIMO
NLOS	Non-Line-of-Sight
OFDM	Orthogonal Frequency-Division Multiplexing
OSIC	Ordered Successive Interference Cancellation
PE	Probability of Error
PEP	Pairwise Error Probability
QAM	Quadrature Amplitude Modulation
RAM	Random Access Memory
SC	Selection Combining
SD	Sphere Decoding
SEP	Symbol Error Probability
SER	Symbol Error Rate
SIMO	Single-Input Multiple-Output
SNR	Signal-to-Noise Ratio
STBC	Space-Time Block Codes

STC	Space-Time Coding
STTC	Space-Time Trellis Codes
SU-MIMO	Single-User MIMO
UE	User Equipment
URLLC	Ultra-Reliable and Low-Latency Communications
VEP	Vector-Symbol Error Probability
VER	Vector-Symbol Error Rate

LIST OF SYMBOLS AND UNITS OF MEASUREMENTS

E_b	Bit energy
N_0	Power spectral density
A_g	Array gain
d	Diversity order
r_{SU}	Single user multiplexing gain
r_{MU}	Multi-user multiplexing gain
N	Number of UEs
N_T	Number of UE's antenna
M	Number of BS's antenna
λ	Load factor
$h(\cdot)$	Channel impulse response
h_{ij}	Complex coefficient impulse response between the jth transmit antenna and the ith receive antenna
$\mathbf{H}$	Channel matrix
$\mathbf{\Psi}$	Receive correlation matrix
$\mathbf{\Sigma}$	Transmit correlation matrix
ρ	Correlation coefficient
$\mathcal{A}$	Modulation order
$\mathcal{M}$	Number of symbols constellation points

INTRODUCTION

Overview

In recent decades, wireless communication systems have undergone significant development, resulting in positive contributions to modern society's economy. The advancements have led to improved throughput, increased connectivity, and enhanced energy efficiency, creating favorable scenarios for developing new applications and connecting more devices.

The fifth generation (5G) wireless communication standard has rapidly deployed worldwide, offering high-speed communication networks with low-latency and massive access (Pavan, Reddy, Prasad, Chintala & Sai, 2023; Yeo, 2023). Meanwhile, current research topics beyond 5G (B5G) networks, known as sixth-generation (6G) networks, aim to offer enhanced connectivity and support more applications than 5G. The research includes network capabilities for various sectors such as industry, autonomous applications, media and entertainment, healthcare systems, virtual and augmented realities, and education (Elijah *et al.*, 2022). B5G is expected to introduce three new scenarios that complement the existing 5G scenarios. These scenarios are ultra-mobile broadband (uMBB), ultra-reliable low-latency broadband communications (ULBC), and massive ultra-reliable low-latency communication (mULC). While the 5G scenarios are massive machine-type communications (mMTC), ultra-reliable and low-latency communications (URLLC), and enhanced mobile broadband (eMBB) communications, the three novel scenarios overlap with them to form an integral set (Pavan *et al.*, 2023; Banafaa *et al.*, 2023; Naeem, Ali, Kaddoum, Huang & Yuen, 2023). Additionally, the technological requirements for B5G implementation will require improvements to existing technologies as well as the incorporation of new ones not considered in 5G. These technologies comprise artificial intelligence (AI) based communication, software centric networks, terahertz communication, ultra-massive antenna arrays, new network topology, and intelligent reflecting surface (IRS) (Kumar, 2022; Naeem *et al.*, 2023).

Multiple-input multiple-output (MIMO) is a technology that deploys multiple antennas at both the transmitter and receiver sides. MIMO can be implemented using either co-located or distributed antennas. Co-located MIMO systems entail antennas placed close to each other, while distributed MIMO systems involve physically separated antennas that may be spread out over a larger area. MIMO systems have many benefits, including improved wireless links in terms of spectral efficiency and reliability. This is due to the multiplexing or diversity gains (Tse & Viswanath, 2006; Björnson, Hoydis & Sanguinetti, 2017). The MIMO channel can be modeled using uncorrelated or correlated Rayleigh fading models. The uncorrelated model assumes an independent fading process between antennas at both ends of the communication link, commonly used in scenarios where antennas are widely separated. In contrast, the correlated Rayleigh fading model considers the correlation between the fading processes of different antennas and is more suitable for scenarios where the antennas are closely located (Tse & Viswanath, 2006).

Multi-user MIMO (MU-MIMO) refers to a system with multiple transmitters or receivers equipped with multiple antennas (Goldsmith, 2005). MU-MIMO is mostly deployed in wireless cellular infrastructures, which include a base station (BS) providing service to multiple user equipments (UE) using the same frequency-time resources (Zhao, Zhao, Zheng & Xiang, 2018).

Massive MIMO, also known as large-scale antenna system, large MIMO, full-dimensional MIMO, large MU-MIMO, or hyper MIMO, is a technology that aims to enhance the benefits provided by conventional MIMO (Marzetta, 2010). In this system, the load factor refers to the ratio between the total number of UEs and the number of receiver antennas at the BS. As the load factor approaches zero, which means that the number of antennas at the BS increases to infinity, the system achieves maximum diversity gain and operates under favorable propagation conditions (Ngo, Larsson & Marzetta, 2014). In contrast, when the load factor is one, also known as the full-load factor, large MU-MIMO enhances the spectral efficiency and achieves a

maximum multiplexing gain. This outcome is particularly desirable in scenarios where a large number of UEs are gathered together close to each other, whether it be in outdoor events, such as "open exhibitions", or in indoor activities where the UEs need to connect to the network, such as a crowded auditorium (Osseiran *et al.*, 2014; Karipidis, 2015).

The detection of large MU-MIMO signals from each UE at the BS is a critical challenge, due to various factors such as channel impairments, interference, and noise. Consequently, researchers and system developers are continuously looking for efficient detection algorithms that strike a good balance between performance and hardware complexity. Linear detectors are low-complexity options that achieve near-optimum performance for large MU-MIMO with low-load factors (Flordelis *et al.*, 2018). However, their performance significantly degrades for moderate and full-load factors due to the assumption of uncorrelated users' channels (Zhang, Wang, Long, Vasilakos & Hanzo, 2015).

On the other hand, non-linear receivers achieve better performance than their linear counterparts at the expense of high hardware complexity, making them impractical solutions. Various detection algorithms based on heuristics, optimization, machine learning, and artificial intelligence have been proposed (Chockalingam & Rajan, 2013). However, their performances are not competitive for a large number of antennas and a high modulation order due to their hardware complexities, which are over an order of magnitude higher than their linear counterparts.

Problem statement

Maximum-likelihood group detection (GD-ML) receivers take a divide-and-conquer approach that achieves a favourable balance between performance and complexity in MIMO systems with a full-load factor. The GD-ML algorithm divides the received symbols into groups and performs the optimum maximum-likelihood (ML) detection on each individual group. GD-ML improves the linear receiver's performance by exploiting the correlation among the channel estimates,

thereby mitigating their interference (Choi, Lee, Shim & Kang, 2013). As a result, it is regarded as an ideal solution for correlated MIMO channels.

In the past decades, there has been extensive research on GD-ML for conventional MIMO systems, focusing on enhancing the structure and grouping strategies. More recently, the GD-ML receiver has emerged as a practical solution for large MU-MIMO systems, as evidenced in (Zhang *et al.*, 2015) and (Nguyen, Le, Ngo, Nguyen & Han, 2018a).

Studies on conventional MIMO and large MU-MIMO systems using the GD-ML technique in the current literature mainly rely on simulation results, where the performance analyses available are limited to idealized channels. These channel models assume a rich scattering Rayleigh fading environment, where the channel matrix entries are independent and identically distributed (i.i.d.). This assumption simplifies the derivation of performance metrics; however, more realistic channel models considering correlated entries, which yield more accurate results and reflect real-world systems, are needed. On the other hand, while the hardware complexity of conventional MIMO is well studied, for large MU-MIMO systems, it still remains unexplored.

The absence of the aforementioned studies has compelled us to establish the research objectives outlined in the following section.

Objectives and Methodology

This thesis aims to assess the efficiency of GD-ML receivers in large MU-MIMO systems. To achieve this goal, two objectives are pursued. The first objective is to develop a computational complexity equation and analyze its efficiency in full-load factor systems by weighing the trade-off between performance and complexity. The second objective is to derive an analytical expression of GD-ML performance for a large MU-MIMO system with a distributed antenna scenario and a correlated channel at the transmitter side.

To achieve these objectives, the following research methodology was adopted:

- Literature Review: Extensive research was conducted on large MU-MIMO receivers, focusing on studying the GD-ML architecture to identify current challenges. The literature review covered the theoretical background of MIMO systems, as well as previous and related works on the structure, complexity, and performance of GD-ML receivers. Multiple research papers, conference proceedings, and relevant textbooks on wireless communication systems were examined to conduct this review.
- System Model: We determined the parameters for a large MU-MIMO system model to establish the target scenario. These parameters include the number of antennas and UEs, antenna distribution, channel model, and modulation scheme.
- Evaluation metrics: We established performance and complexity metrics to evaluate the studied receivers. The performance assessment comprises the bit error rate (BER) and vector-symbol error rate (VER), while the complexity is measured through floating-point operations (FLOPs), considering the number of UEs and antennas at the BS.
- Mathematical Analysis: We formulated analytical equations to evaluate the performance and complexity of GD-ML receivers based on the defined metrics. Our methodology involves utilizing multivariate random theory and stochastic ordering to derive the performance expressions. We analyzed the matrix operations involved in each stage of the GD-ML receiver structure to determine its complexity in FLOPs. The resulting derivations were then compared with simulations in Matlab.

Contributions

Based on the proposed objectives and methodology, this thesis makes new contributions to the GD-ML performance and complexity analysis by taking into account correlated MU-MIMO channels and a large number of distributed antennas at the BS. These contributions are summarized as follows:

- We derive a closed-form expression of the average group VER for large MU-MIMO systems with correlated channels at the transmitter-side and negligible correlation at the receiver-side, suitable for scenarios with a large number of closely-located UEs and a massive number of distributed BS antennas. The derived analytical expression is based on multivariate complex random variables and stochastic order theory.
- We derive a formula for the hardware complexity of GD-ML receiver for full-load large MU-MIMO systems and provide a comparison analysis with the linear receivers counterparts in terms of complexity-performance compromise. The complexity expression is stated in terms of FLOPs in relation to the number of UEs and the group size.

Thesis organization

The remainder of this thesis is organized as follows:

- Chapter 1 presents an overview of wireless communication systems, which includes the fading phenomena and its mitigation. Moreover, we provide a review of MIMO systems, which includes the diversity and spatial multiplexing techniques, the MU-MIMO, and large MIMO systems. Then, a review of MU-MIMO detection is boarded, where the performance and complexity of linear and non-linear algorithms are compared. We finish this chapter by presenting the structure, complexity analysis, and numerical results of the GD-ML receiver.
- Chapter 2 provides the literature review of GD-ML techniques for MIMO systems. The review works on the receiver structure, grouping strategies, and performance analysis.
- Chapter 3 describes the mathematical procedure for deriving the analytical expression of the average VER of the GD-ML receiver, as well as the validation of this expression using simulation results. This is one of the main contribution of this research work.
- Finally, we provide the conclusions based on the obtained results and summarizes the benefits of GD-ML. We also propose future works to extend the current research.

CHAPTER 1

BACKGROUND OF SPATIAL MULTIPLEXING SYSTEMS

1.1 Overview

In this chapter, we provide the essential concepts of MIMO systems, their variants, and their benefits, with an emphasis on the description of classic detection techniques and the alternative group detection algorithm. To this end, this chapter is divided into six sections. In Section 1.2, we provide an overview of wireless communication systems, with a focus on wireless networks, fading, and diversity. MIMO systems are introduced in Section 1.3, which describes spatial multiplexing and diversity techniques as well as their array, diversity, and multiplexing gains. In addition, the section includes the study of MU-MIMO and large MU-MIMO systems. Section 1.4 presents an overview of MIMO channel models and correlated MU-MIMO mathematical model. Classical MU-MIMO detection is provided in Section 1.5, where linear and non-linear receivers are discussed in terms of performance and complexity. Finally, the structure, complexity analysis, and numerical results of the GD-MLtechnique are presented in Section 1.6.

1.2 Wireless communications systems

A communication system deals with the information interchange from one point to another. The essential elements of this system are the *message*, *transmitter*, *receiver*, and *channel*. The message is the information or data to be sent; the transmitter and receiver are the electronic devices that transmit and receive the information, respectively; the channel is the medium of transmission, which can be wired or wireless (Dalal, 2021).

A wireless communication system is a system in which the information is modulated and transmitted over radio waves through a wireless channel by either line-of-sight (LOS) or non-line-of-sight (NLOS) links. There are three types of wireless communication systems: *wireless networks*, which are communications systems that allow the endpoints to exchange information independently, being a transmitter or receiver; the *wireless broadcast systems*, which provide

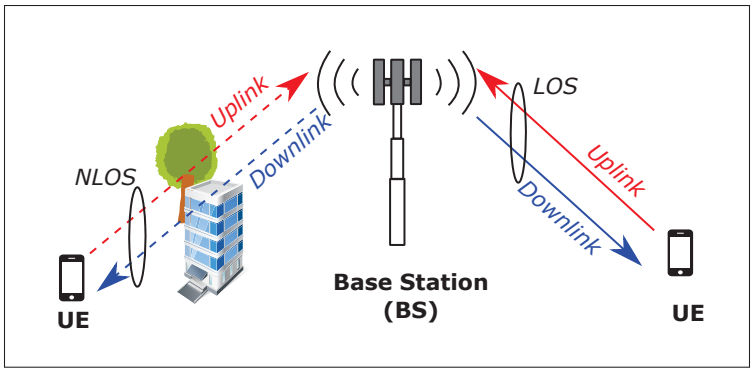

Figure 1.1 Cellular wireless network

the simultaneous communication between a single transmitter and multiple receivers; *wireless navigation systems*, which provide a location-based service supported by the global positioning system and the Internet (Dalal, 2021). In this thesis, we only consider wireless network systems.

1.2.1 Wireless Networks

Wireless networks are based on ad hoc connections or cellular infrastructure (Dalal, 2021). Ad hoc networks allow all users to be transmitters, receivers, or relays for other users' communications. On the other hand, cellular infrastructure is characterized by a centralized communication system with a BS providing service to multiple UEs, sharing frequency-time resources, where the BS controls the data transmission and reception procedures.

Wireless networks operate over a multi-user channel, which refers to a channel shared by multiple users. This channel is divided into the *uplink* and *downlink* channels, described below (Goldsmith, 2005).

a. The *downlink channel*, known as broadcast channel (BC) or forward channel, involves one transmitter sending information to many receivers, which corresponds to the communications between the BS to UEs in a cellular structure.
b. The *uplink channel*, called multiple access channel (MAC) or reverse channel, involves multiple transmitters sending signals to one receiver, where each signal shares the total

system bandwidth, e.g., the transmissions from UEs to a BS, wireless LAN access point receiving information from all connected users.

Figure 1.1 shows a cellular wireless network, illustrating some concepts presented above.

1.2.2 Fading

Due to the physical nature of wireless channels, which can be the atmosphere or free space between the transmitter and receiver, the transmitted signal can be affected by three phenomena: reflection, diffraction, and scattering (Cho, Kim, Yang & Kang, 2010). These events create a multipath propagation environment, with the reception of multiple copies of the transmitted signal.

Fading is a wireless channel perturbation that causes severe degradation in the performance and reliability of wireless communication systems. Fading can be defined as a non-additive random fluctuation of the transmitted signal in amplitude and phase. This random phenomenon is commonly characterized by the Rician and Rayleigh distributions for LOS and NLOS channels, respectively.

Fading can be classified into large-scale fading and small-scale fading, which are illustrated in Figure 1.2 and described below (Cho *et al.*, 2010):

a. Large-scale fading is a signal degradation due to a path loss as a function of distance and shadowing caused by large objects between the transmitter and receiver.
b. Small-scale fading is defined as fast signal variations due to interference caused by multipath propagation when the user moves short distances, which can be characterized as frequency-selective or frequency-flat channels (Cho *et al.*, 2010). Small-scale fading can also be generated by the time variation in a channel due to the user's speed, also called Doppler spread, resulting in fast fading or slow fading (Rappaport, 2002).

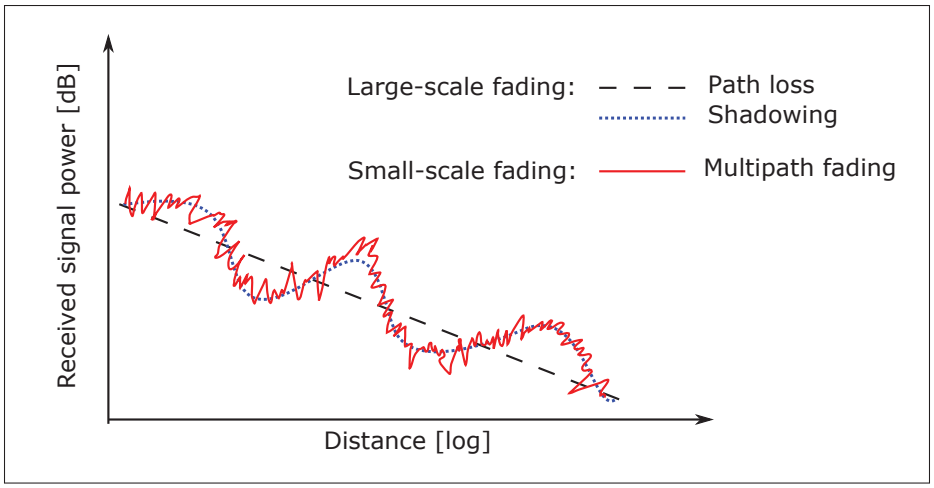

Figure 1.2 Relation between large-scale fading and small-scale fading
Adapted from Cho et al. (2010, p.3)

1.2.3 Diversity: fading mitigation technique

Diversity is a technique for mitigating fading, which implies using many statistically independent copies of the information signal over different times, frequencies, or spaces to enhance the reliability of the wireless communication system. There are many ways of achieving diversity gains, including the following configurations (Tse & Viswanath, 2006; Cho *et al.*, 2010):

a. *Time diversity*: many copies of the same information signals are transmitted over multiple time slots.

b. *Frequency diversity*: the same information is repeatedly transmitted in multiple spectral bands.

c. *Space diversity*: implies the use of multiple antennas sufficiently separated to generate independent wireless channels through which multiple information signal replicas are either transmitted or received, also called *antenna diversity*. Various antenna configurations such as MIMO, multiple-input single-output (MISO), and single-input multiple-output (SIMO) are space diversity techniques.

Time and frequency diversities require additional time and spectrum resources compared to space diversity (Cho *et al.*, 2010). Besides improving wireless system reliability, MIMO systems

also enhance the communication system's capacity without increasing the power and bandwidth resources.

1.2.4 System performance and hardware complexity measures

In this section, we address the description of the main system's performance evaluation methods as well as the description of the used computational complexity metric.

1.2.4.1 Probability of error

The probability of error (PE) can be defined as a disagreement between the transmitted and detected message (Proakis & Salehi, 2008). The PE includes three types: bit error probability (BEP), which measures errors in transmitting a single bit; symbol error probability (SEP), which refers to errors in transmitting a symbol or a message (Proakis & Salehi, 2008); and vector-symbol error probability (VEP) assesses the PE in comparing the transmitted and received user's symbol vectors.(Talwar & Paulraj, 1997; Jiang & Liu, 2021).

The PE as a function of the signal-to-noise ratio (SNR), denoted as $PE(SNR)$, is the natural benchmark for evaluating communication systems' performance. The PE is usually a curve that shows how the system's performance changes with varying the SNR. As the SNR increases, the PE decreases since the received signal is stronger and less susceptible to noise-induced errors. In digital wireless communication systems, the receivers' performance is often measured by the average PE as a function of the ratio of bit energy to noise power spectral density E_b/N_0, denoted as $\overline{PE}(E_b/N_0)$. The term average refers to statistical averaging over the probability distribution channel effects (Sklar & Kumar, 2017), and the E_b/N_0 is a normalized version of SNR.

Deriving a closed-form expression of the average PE becomes difficult because it is a non-linear function of the instantaneous SNR and the modulation-detection mechanism utilized by the system (Simon & Alouini, 2000). Thus, various upper and lower bounds on the PE are useful approaches. The upper bound describes the worst-case scenario of the receiver's performance scenario, while the lower bound analyzes the best-case scenario (Stüber, 2011). Finally, the

pairwise error probability (PEP) is a useful method to determine the upper or lower bounds, which refers to the probability that a specific pair of transmitted messages will be incorrectly detected at the receiver (Stüber, 2011; Simon & Alouini, 2000).

The bit error rate (BER), symbol error rate (SER), and vector-symbol error rate (VER) are performance metrics used in the literature as alternatives to the PE (Simon & Alouini, 2000; Talwar & Paulraj, 1997). Instead of choosing a preference, we use these terms interchangeably in this thesis. The BER, SER, and VER are the ratios of incorrectly transmitted bits, symbols, and vector-symbol to all transmitted bits, symbols, and vector symbols, respectively, over a given time period. They are commonly used in the performance simulation of digital communications systems.

1.2.4.2 System capacity

The system capacity refers to the maximum amount of messages that can be transmitted through the system (Tse & Viswanath, 2006). The capacity is a common metric to evaluate the system's rate, typically a function of SNR, denoted as $C(SNR)$, measured in bits per second (bps) used to measure the system's data transmission rate.

1.2.4.3 Hardware complexity metric

Computational complexity in digital receivers refers to the amount of computational resources, such as CPU and RAM, required to perform the signal processing tasks involved in detecting the transmitted messages. These tasks include matrix products and inverses of matrices performed by digital computers. A FLOP is a mathematical operation performed on floating-point numbers in computer programming that represents the number of multiplications and summations required to solve matrix-vector operations (Hunger, 2007). In this thesis, we use the number of FLOPs to measure the hardware complexity required to perform the detection algorithms, in addition to the use of the big O notation $\mathcal{O}[\cdot]$. Table 1.1 displays the FLOPs needed for the matrix operations that are commonly used in signal detection.

Table 1.1 FLOPs required for mathematical operations
for $\alpha \in \mathbb{C}$, $\mathbf{A} \in \mathbb{C}^{M \times N}$, $\mathbf{B} \in \mathbb{C}^{N \times N}$, $\mathbf{a}, \mathbf{b} \in \mathbb{C}^{N}$, and
$\mathbf{R} \in \mathbb{C}^{N \times N} > 0$
Adapted from Hanger (2007, p. 14)

Expression	Description	FlOPs
$\alpha\mathbf{a}$	Vector scaling	N
$\alpha\mathbf{A}$	Matrix scaling	NN
$\mathbf{a}^H\mathbf{b}$	Inner product	$2N-1$
$\mathbf{AB}$	Matrix vector product	$2MN-M$
$\mathbf{A}^H\mathbf{A}$	Gram	$MN^2+N\left(M-\frac{N}{2}\right)-\frac{N}{2}$
$\parallel \mathbf{A} \parallel_F^2$	Frobenius norm	$2MN-1$
$\mathbf{a}^H\mathbf{Ra}$	Hermitian form	$\frac{3}{2}N^2+\frac{3}{2}N-1$
$\mathbf{R}^{-1}$	Inverse	$2N-1$
-	Sequential access	N

1.3 MIMO systems

MIMO, or single-user MIMO (SU-MIMO), is a communication technology that employs N_T and M antennas at the transmitter and receiver sides, respectively. The information symbols are processed to enhance either the reliability or throughput of the wireless communication system by exploiting the multipath propagation of the MIMO channel.

The distribution of the BS antennas significantly impacts the system's performance. Thus, there are two BS antennas distribution layouts: co-located antenna and distributed antenna systems, as shown in Figure 1.3.

a. *Co-located antennas:* In co-located antenna systems, the antennas are positioned at the BS with a typical half-wavelength spacing to mitigate the spatial correlation. Conventionally, the BS is placed in the centre of the cell, and the antenna array is at the tower's top. However, this configuration adds some challenges to the detection design due to the correlated channels at the BS, even when the antennas are well separated (Zhao *et al.*, 2018; Kamga, Xia & Aïssa, 2016).

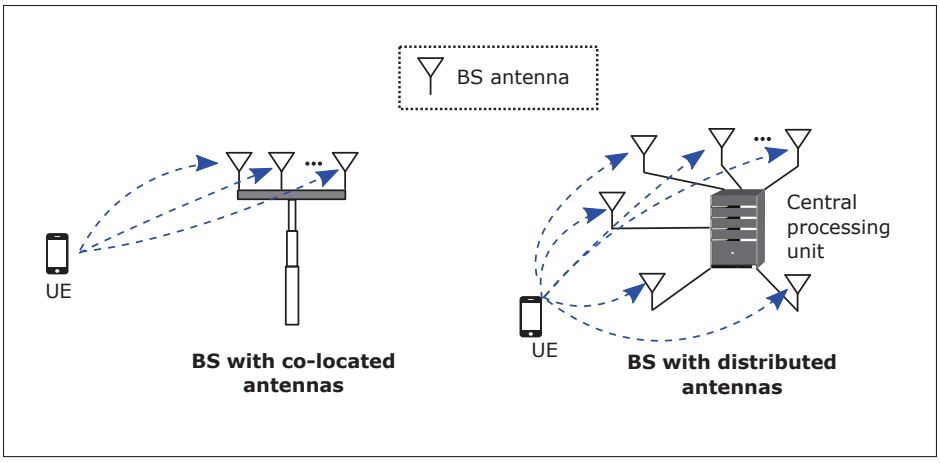

Figure 1.3 BS antenna distribution layouts
Adapted from Kamga et al. (2016, p. 1931)

b. *Distributed antennas:* In contrast to co-located antenna systems, here the BS antennas are placed in different geographical locations and connected to a central processing unit. The main advantage of distributed systems is that they perform better than their co-located antenna counterparts because the signals arriving from UEs to the BS are subject to independent fading (Zhao *et al.*, 2018). Since the antennas at the BS are well separated, the correlation between them is negligible (Kamga *et al.*, 2016).

In real communication systems, distributed and co-located antennas may be considered complementary rather than competitive technologies (Kamga *et al.*, 2016).

1.3.1 MIMO techniques

MIMO techniques can be classified in diversity and spatial multiplexing. The diversity scheme increases the system's performance, and spatial multiplexing enhances the system's rate.

1.3.1.1 Diversity technique

Diversity implies the transmission or reception of multiple replicas of the information symbols, increasing the number of independent channel paths to mitigate the fading effects, thereby

enhancing the system's performance (Cho *et al.*, 2010). This feature is equivalent to converting the fluctuating wireless fading channel into a more stable channel. Diversity provides array and diversity gains, which are described in the following:

a. **Array gain**, denoted as A_g, is defined as the increase of the SNR at the receiver side, thereby improving the range and coverage of the wireless cellular network. It is expressed as

$$A_g = \frac{\overline{SNR}}{\overline{SNR}_b}, \tag{1.1}$$

where $\overline{SNR}$ is the average combined SNR and $\overline{SNR}_b$ is the average branch SNR (Goldsmith, 2005).

b. **Diversity gain**, also called *diversity order*, denoted as d, is the number of independent channel realizations over which the information is transmitted. The maximum diversity order that can be achieved is MN_T, where the system is said to achieve full diversity order.

The diversity order determines how the slope of $PE(SNR)$ changes with diversity in a log-log scale at high SNR, expressed as (Goldsmith, 2005)

$$d = -\lim_{SNR\to\infty} \frac{\log PE(SNR)}{\log(SNR)}. \tag{1.2}$$

Furthermore, the PE over Rayleigh fading channels can be expressed as

$$PE(SNR) \propto \frac{1}{SNR^d}, \tag{1.3}$$

which means that increasing the diversity order enhances the system's performance causing an exponential fall in the PE (Chockalingam & Rajan, 2013).

There are two technologies associated for achieving diversity: beamforming and space-time coding.

a. **Beamforming**

Beamforming requires knowledge of the channel state information (CSI) and implies precoding and combining operations involving the use of weight factors at the transmitter

and receiver sides, respectively. *Precoding* implies the same information signal is scaled by the weight factor and transmitted by each antenna, e.g., maximum ratio transmission (MRT). In contrast, the *combining* operation applies the weight factor to the signals received at each antenna on the receiver side (Goldsmith, 2005). Combining algorithms include selection combining (SC), maximum ratio combining (MRC), and equal gain combining (EGC). SC selects the received signal with the highest SNR value. In contrast, MRC combines all received signals with the appropriate weight factors to maximize the post-combining SNR. Finally, EGC can be considered as a special case of MRC, which uses the same weight factors for all received signals (Chaudhari, 2021; Goldsmith, 2005; Cho *et al.*, 2010).

b. **Space-Time Coding**

Space-time coding (STC) is a diversity technique based on constructing a code from information symbols and its transmission at different time intervals across multiple antennas. STC requires multiple transmit antennas, while only a single antenna is needed for the receiver. However, multiple receive antennas improve the diversity gain. STC can be classified into space-time block codes (STBC) and space-time trellis codes (STTC).

STBC encode the information symbols with orthogonal blocks usually represented by a matrix in which the rows represent time slots and the columns the antenna transmissions, thereby providing diversity gain. The blocks are orthogonal if any pair-wise columns are orthogonal. The attractive feature of orthogonal STBC is that linear processing decoding can achieve the optimal performance. The Alamouti scheme is the most popular orthogonal STBC algorithm. On the other hand, the STTC scheme transmits multiple redundant copies of generalized trellis-coded modulation (TCM) symbols distributed across all transmit antennas and time. Besides the diversity gain, STTC provide coding gain and better performance compared to STBC, at a hither complexity cost due to the Viterbi decoder (Goldsmith, 2005; Cho *et al.*, 2010).

1.3.1.2 Spatial Multiplexing

Spatial multiplexing technique simultaneously transmit independent information symbols from each transmit antenna, providing a linear increase in the available data rate. Thus, for a well-conditioned MIMO system, i.e., $M \geq N_T$, the multiplexing gain, also known as degrees of freedom, is given by (Tse & Viswanath, 2006)

$$r_{\text{SU}} = \min\{M, N_T\}. \tag{1.4}$$

The multiplexing gain can also be interpreted as the slope of the system capacity as a function of SNR at high SNR in log scale, and is expressed as Goldsmith (2005)

$$r = \lim_{SNR \to \infty} \frac{\log C(SNR)}{\log(SNR)}. \tag{1.5}$$

At the receiver side, the spatial demultiplexing process or signal detection is challenging due to inter-streams interference. Thus, for reliable detection of the received data streams, the basic requirement is that the number of receive antennas must be greater than or equal to the number of transmit antennas; then, both linear and non-linear detectors are able to demultiplex the transmitted symbols and eliminate the multi-streams interference subject to trade-off between the performance and complexity cost.

1.3.2 Multi-user MIMO systems

A multi-user MIMO (MU-MIMO) system is a wireless communication network with multiple transmitters or receivers equipped with multiple antennas (Goldsmith, 2005), which is an improvement over SU-MIMO technology. We consider a typical cellular wireless network with N UEs with N_T antennas, resulting in a virtual $N \cdot N_T$ antenna array, served by a single BS equipped with M antennas (Cho *et al.*, 2010).

1.3.2.1 Uplink and downlink MU-MIMO systems

As mentioned earlier, multi-user communications are performed over uplink and downlink channels. Thus, there are two environments associated with MU-MIMO.

a. *Uplink* MU-MIMO: The $M \times (N \cdot N_T)$ uplink MU-MIMO system, also known as multiple access MIMO (MIMO-MAC), enables the UEs to transmit their signals at the same frequency-time resources without multi-user signal processing. The BS decodes the cumulative signal using multi-user detection algorithms with knowledge of the CSI. Let's note that if all N UEs are equipped with a single antenna, the resulting MU-MIMO system is equivalent to an SU-MIMO system (Cho *et al.*, 2010).
b. *Downlink* MU-MIMO: The $(N \cdot N_T) \times M$ downlink MU-MIMO system, also called broadcast MIMO (MIMO-BC), allows the BS to transmit signals to each UE using the beamforming technique, which sums the weighted signals of the N users before transmitting the output signal from the M BS antennas. This procedure requires full CSI knowledge at the BS (Chaudhari, 2021).

1.3.2.2 Diversity and multiplexing gains of MU-MIMO

The diversity and spatial multiplexing techniques, presented for SU-MIMO apply to MU-MIMO systems as well, offering diversity and multiplexing gains that improve the communication system's performance and capacity. These benefits are described below:

a. Spatial multiplexing allows multiple UEs to be simultaneously served by the BS, enhancing the uplink and downlink capacity proportional to the multiplexing gain, as given by (Goldsmith, 2005; Cho *et al.*, 2010)

$$r_{\text{MU}} = \min(N \cdot N_T, M). \tag{1.6}$$

We can observe that the multiplexing gain of SU-MIMO given in (1.5) is limited by the minimum number of transmit and receive antennas. This affirmation shows that the multiplexing gain of MU-MIMO can be achieved even with single antenna UEs, as shown in 1.6.

b. The diversity gain in MU-MIMO systems can be achieved based on the schedule or allocation process. These processes consider the CSI to select the appropriate UEs to access the system resources and transmit the data on specific spatial streams or transmit antennas. The main advantage of this strategy is that the linear transmitters and receivers can achieve near-optimal performance as the number of UEs increases (Goldsmith, 2005). In SU-MIMO, the beamforming technique provides diversity gain at the cost of of reduced overall system capacity since it cannot fully exploit the available antennas for parallel data transmission. However, beamforming for downlink MU-MIMO achieves diversity gain proportional to N_T, and also achieves the sum capacity rate (Goldsmith, 2005; Tse & Viswanath, 2006).

1.3.3 Large MU-MIMO systems

Large MU-MIMO is an extension of MU-MIMO systems with hundreds of antennas at the end points, thereby increasing the multiplexing and diversity gains. In this scenario, the greater the number of antennas, the greater the degrees of freedom of the system (Marzetta, 2010; Chockalingam & Rajan, 2013).

In a typical wireless network with a MU-MIMO system, UEs are usually small devices with a limited the number of antennas, while the BS is a robust physical infrastructure. Hence, the signal processing and hardware cost are assigned to the BS, while UEs are kept as simple as possible. For these reasons, in this thesis, we consider a large MU-MIMO system with single-antenna UEs and a BS with a large number of antennas.

Let's define the load factor as the ratio of the total number of UEs to the number of receive antennas at the BS as

$$\lambda = \frac{N}{M}, \tag{1.7}$$

where $\lambda \in (0, 1]$, resulting in two main scenarios: canonical massive MIMO and full-load large MU-MIMO.

a. Canonical massive MIMO is considered when the load factor approaches zero, i.e., the number of antennas at the BS increases to infinity. Thus, the system operates in a favourable

propagation condition and channel hardening (Björnson, Hoydis, Kountouris & Debbah, 2014). These conditions theoretically allow low-complexity linear detectors to achieve near-optimum performance in the uplink and use simple precoding algorithms and flexible user selection and scheduling for downlink connections (Chockalingam & Rajan, 2013).

b. Full-load large MU-MIMO is a system with equal numbers of UEs and antennas at the BS; thus, $\lambda = 1$. This scenario provides a maximum multiplexing gain allowing a large number of UEs to access the system. In this scenario, linear detectors no longer offer near-optimum performance due to the unitary diversity gain (Mandloi, Gurjar, Pattanayak & Nguyen, 2021).

1.4 MU-MIMO channel

Let $h(t, \tau)$ denote as the time-variant impulse response of the channel between the transmitter and receiver for a single antenna system, where t and τ stand for time and delay, respectively. For a time-invariant channel, the impulse response can be written as $h(\tau)$, in which the dependence on time vanishes. Furthermore, the impulse response of the time-invariant and frequency-flat channel does not depend on time, and only one single tap is required; thus, it can be denoted by h (Darbari, Stewart & Glover, 2010).

In this thesis, we consider time-invariant and frequency-flat uplink MU-MIMO channel with a BS equipped with M antennas serving N UEs with a single antenna. In this scenario, the channel is composed of all pairs of transmit and receive antennas forming an $M \times N$ channel matrix expressed as

$$\mathbf{H} = \begin{pmatrix} h_{11} & h_{12} & \cdots & h_{1N} \\ h_{21} & h_{22} & \cdots & h_{2N} \\ \vdots & \vdots & \ddots & \vdots \\ h_{M1} & h_{M2} & \cdots & h_{MN} \end{pmatrix}, \tag{1.8}$$

where h_{ij} is a complex coefficient impulse response between the jth transmit antenna and the ith receive antenna. Many channel models have been proposed to determine these coefficients, which can be widely classified into physical and analytical models (Almers *et al.*, 2007):

a. The physical models characterize the channel coefficients based on electromagnetic wave propagation, which describes the double-directional multipath between the transmitter and the receiver. These models consider channel parameters, such as complex amplitude, the direction of departure (DoD), the direction of arrival (DoA), and the delay of the multipath components. Physical models are able to provide an accurate representation of radio propagation at the cost of a high computational complexity. However, these models do not consider the antenna configuration, such as the number of antennas, array geometry, antenna pattern, polarization, and system bandwidth. Examples of physical models include ray tracing, stored measurement data, and the Saleh-Valenzuela model (Almers *et al.*, 2007).
b. Analytical models characterize the channel impulse response coefficients between the individual transmit and receive antennas with a mathematical model without explicitly considering wave propagation. The resulting channel matrix is widely used for communication system evaluation. Analytical models can be divided into propagation-motivated models and correlation-based models. The propagation-motivated models generate the channel matrix based on propagation parameters, such as DoA, delay, etc. Examples of analytical models include virtual channel representations, maximum entropy, and finite scatterer. Correlation-based models consider the correlation between the entries of the channel matrix, which are statistically generated (Chockalingam & Rajan, 2013). Popular models include the Kronecker model and the Weichselberger model.

1.4.1 Correlation-based model

In this model, the correlation between the entries of the channel matrix can be divided into two types: transmit correlation, which represents the correlation between UEs' channels, and receive correlation representing the correlation between antennas at the BS. We consider the Kronecker model, where the transmit and receive correlation can be represented by separable matrices. Thus, the channel matrix, given in (1.8), can be represented by

$$\mathbf{H} = \mathbf{\Psi}^{1/2}\mathbf{H}_{\mathrm{w}}\mathbf{\Sigma}^{1/2}, \tag{1.9}$$

where $\mathbf{\Psi} \in \mathbb{C}^{M\times M} > \mathbf{0}$ and $\mathbf{\Sigma} \in \mathbb{C}^{N\times N} > \mathbf{0}$ are the receive and transmit correlation matrices, respectively. $\mathbf{H}_{\text{w}} \in \mathbb{C}^{M\times N}$ is an $(M \times N)$-complex random matrix-variate Gaussian distribution with zero-mean matrix $\mathbf{0} \in \mathbb{C}^{M\times N}$ and covariance matrix $\mathbf{I}_M \otimes \mathbf{I}_N$ denoted as $\mathbf{H}_{\text{w}} \sim \mathbb{C}\mathcal{N}_{M,N}(\mathbf{0}, \mathbf{I}_M \otimes \mathbf{I}_N)$ (for further details, refer to Annex I), which represents the i.i.d. (independent and identically distributed) Rayleigh-fading channel (Cho *et al.*, 2010; Shin & Lee, 2003). Moreover, $(\mathbf{H}_{\text{w}})_{ij} \sim \mathbb{C}\mathcal{N}_1(0, 1)$ is a zero-mean complex univariate Gaussian random variable with unit covariance, and $(\cdot)_{ij}$ denotes the (ij)-th entry of matrix $\mathbf{H}_{\text{w}}$.

The channel matrix in (1.9) is also defined as an $(M \times N)$-complex random matrix-variate Gaussian distribution with zero-mean matrix $\mathbf{0} \in \mathbb{C}^{M\times N}$, and covariance matrix $\mathbf{\Psi} \otimes \mathbf{\Sigma}$, expressed as (Shin & Lee, 2003)

$$\mathbf{H} \sim \mathbb{C}\mathcal{N}_{M,N}(\mathbf{0}, \mathbf{\Psi} \otimes \mathbf{\Sigma}). \tag{1.10}$$

Let's remark that if $\mathbf{\Psi} = \mathbf{I}_M$ and $\mathbf{\Sigma} = \mathbf{I}_N$, the channel matrix $\mathbf{H} = \mathbf{H}_{\text{w}}$, which implies that the channel is uncorrelated.

1.4.1.1 Receive correlation matrix

The exponential correlation model is considered a reasonable approximation for antennas at the BS with a uniform linear array (ULA). In this model, the correlation between two antenna elements exponentially decreases by increasing the distance between them (Loyka, 2001; Razi, Ryan, Yuan & Collings, 2010). The entries of the $M \times M$ receive correlation matrix $\mathbf{\Psi}(\rho_r)$, which is a Hermitian Toeplitz matrix, are given by

$$(\mathbf{\Psi}(\rho_r))_{jk} = \rho_r^{|k-j|}, \tag{1.11}$$

where $\rho_r \in [0, 1]$ is the receive correlation coefficient and $j, k = 1, \cdots, M$.

1.4.1.2 Transmit correlation matrix

We now consider a constant correlation matrix for closely-located and correlated UEs in dense networks (Shin & Lee, 2003). An $N \times N$ correlation matrix, also called Nth-order positive-definite, can be expressed as (Gao, Jiang, Li, Gershman & McKay, 2009)

$$\mathbf{\Sigma}(\rho_t) = \rho_t \mathbf{1}_N + (1 - \rho_t)\mathbf{I}_N, \tag{1.12}$$

where $\mathbf{1}_N$ is an $(N \times N)$ matrix with all entries equal to one. Also, in (1.12), $\rho_t \in [0, 1]$ is the transmit correlation coefficient, given by

$$\rho_{t_{(i_1 i_2)}} = \langle |h_{ji_1}|^2, |h_{ji_2}|^2 \rangle, \tag{1.13}$$

where $h_{ji_k} = (\mathbf{H})_{ji_k}$, $k = 1, 2$ denotes entries of the channel $\mathbf{H}$ given in (1.9), and

$$\langle x, y \rangle = \frac{\mathbb{E}\{xy\} - \mathbb{E}\{x\}\mathbb{E}\{y\}}{\sqrt{(\mathbb{E}\{x^2\} - \mathbb{E}\{x\}^2)(\mathbb{E}\{y^2\} - \mathbb{E}\{y\}^2)}}, \tag{1.14}$$

which is a model that can be used for worst-case analysis.

1.5 MU-MIMO detection

Signal detection at the BS receiver is the most challenging task of the spatial multiplexing technique in the uplink MU-MIMO system. The main goal of the detection is to estimate the transmitted information from all UEs transmitting at the same frequency-time resources. In the literature, linear and nonlinear detectors are the main detection algorithms whose performances are subject to computational complexity. Hence, the detection algorithms' main challenge is to achieve a good trade-off between performance and complexity, which is an area of continuous research.

This section presents the system model and the optimum MU-MIMO receiver is considered as a reference when evaluating the remaining detection algorithms. Then, we discuss classic linear

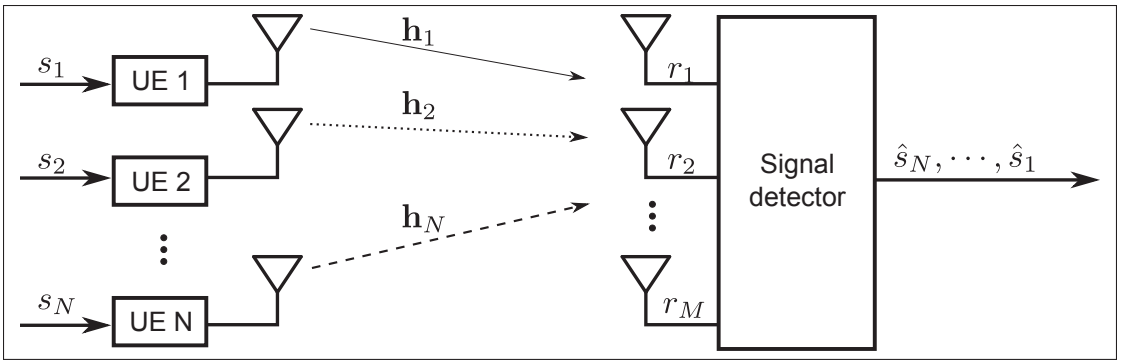

Figure 1.4 Uplink spatial multiplexing system

receiver algorithms and briefly describe non-linear receivers. Finally, we present numerical results of linear receivers' performance a comparison of the complexity of the described detection algorithms.

1.5.1 System model

We consider an uplink large MU-MIMO system with M receive antennas at the BS and N single antenna UEs, as shown in Figure 1.4. The transmitted symbols vector from all UEs is denoted by $\mathbf{s} \in \mathbb{C}^N$, which has a zero-mean and matrix covariance $\mathbb{E}[\mathbf{s}\mathbf{s}^H] = \mathbf{I}_N$. The entry $s_i \in \mathbf{s}$, for $i = 1, \cdots, N$ is the transmitted symbol from the ith user, which is a complex modulated signal of modulation order $\mathcal{A}$. The equivalent received complex signal vector is denoted as $\mathbf{r} \in \mathbb{C}^M$, where the entry $r_j \in \mathbf{r}$, $j = 1, \cdots, M$, represents the received signal at the jth antenna. The vector $\mathbf{r}$ can be expressed as (Maza, Dahman, Kaddoum & Gagnon, 2020)

$$\begin{aligned} \mathbf{r} &= \sum_{i=1}^{N} \mathbf{h}_i s_i + \mathbf{n} \\ &= \mathbf{H}\mathbf{s} + \mathbf{n}, \end{aligned} \tag{1.15}$$

where $\mathbf{n} \in \mathbb{C}^M \sim \mathbb{C}\mathcal{N}_M(\mathbf{0}, \sigma_n^2 \mathbf{I}_M)$ is defined as the zero-mean complex M-variate Gaussian vector with covariance matrix $\sigma_n^2 \mathbf{I}_M$, and σ_n^2 is the complex noise variance. Moreover, $\mathbf{h}_i \in \mathbb{C}^M$ is the ith user's channel vector, and $\mathbf{H} \in \mathbb{C}^{M \times N}$ is the multiple-access channel matrix given in (1.9),

which is assumed to be known at the receiver side. Then, the complex channel coefficients are given by

$$(\mathbf{H})_{ji} = h_{ji}, \tag{1.16}$$

where, h_{ji}, $j = 1, \cdots, M$ and $i = 1, \cdots, N$ denotes the complex channel coefficient between the ith UE and the jth receiver antenna at the BS.

1.5.2 Optimum receiver

The detection procedure estimates the transmitted vector, $\mathbf{s}$, from the received vector $\mathbf{r}$ given in (1.15). The optimum receiver chooses the candidate $\hat{\mathbf{s}}$ from the constellation $\mathcal{A}^N$ that minimizes the PE, denoted as

$$PE \triangleq \Pr\{\hat{\mathbf{s}} \neq \mathbf{s}\}, \tag{1.17}$$

which is equivalent to maximizing the probability of correct decision given $\mathbf{r}$, expressed as (Proakis & Salehi, 2008)

$$\Pr\{\hat{\mathbf{s}} = \mathbf{s}|\mathbf{r}\} = \frac{f(\mathbf{r}|\mathbf{s} = \hat{\mathbf{s}})\Pr\{\hat{\mathbf{s}} = \mathbf{s}\}}{f(\mathbf{r})}, \tag{1.18}$$

where $f(\mathbf{r})$ is the probability density function (PDF) of the received vector $\mathbf{r}$ and $f(\mathbf{r}|\mathbf{s} = \hat{\mathbf{s}})$ is the PDF of $\mathbf{r}$ when the transmitted vector is $\hat{\mathbf{s}}$. Since $f(\mathbf{r})$ does not depend on $\hat{\mathbf{s}}$, the optimum receiver obtains $\hat{\mathbf{s}}$ maximizing the a posteriory probability

$$\hat{\mathbf{s}} = \arg \max_{\mathbf{s} \in \mathcal{A}^N} f(\mathbf{r}|\mathbf{s} = \hat{\mathbf{s}})\Pr\{\hat{\mathbf{s}} = \mathbf{s}\}. \tag{1.19}$$

Then, if the transmitted symbols are equiprobable, (1.19) is equivalent to the estimated symbols vector given by the ML detector algorithm, expressed as

$$\hat{\mathbf{s}}_{\text{ML}} = \arg \max_{\mathbf{s} \in \mathcal{A}^N} f(\mathbf{r}|\mathbf{s} = \hat{\mathbf{s}}). \tag{1.20}$$

From (1.15), we get (Barry, Lee & Messerschmitt, 2004)

$$f(\mathbf{r}|\mathbf{s} = \hat{\mathbf{s}}) = f(\mathbf{n}). \tag{1.21}$$

Substituting $\mathbf{n} = \mathbf{r} - \mathbf{Hs}$, the PDF of the white Gaussian noise $\mathbf{n}$ is given by

$$f(\mathbf{n}) = \frac{1}{(\pi\sigma^2)^N} e^{-\frac{1}{\sigma^2}\|\mathbf{r}-\mathbf{Hs}\|^2}. \tag{1.22}$$

From (1.21) and (1.22), we can conclude that maximizing $f(\mathbf{r}|\mathbf{s} = \hat{\mathbf{s}})$ is equivalent to minimizing $\| \mathbf{r} - \mathbf{Hs} \|^2$. Thus, (1.20) can be rewritten as

$$\hat{\mathbf{s}}_{\text{ML}} = \arg\min_{\mathbf{s}\in\mathcal{S}} \| \mathbf{r} - \mathbf{Hs} \|^2, \tag{1.23}$$

where $\mathcal{S}$ is the set of symbols constellation points with $\mathcal{M} = \mathcal{A}^N$ elements. Hence, the ML detector achieves the optimum detection by choosing the vector $\hat{\mathbf{s}}$ that produces the smallest Euclidean distance between $\mathbf{r}$ and $\mathbf{Hs}$ at the complexity cost of $O[\mathcal{M}]$.

1.5.3 Linear detection

Linear detection is a low-complexity algorithm that theoretically achieves near-optimum performance for large MU-MIMO systems with $\lambda \ll 1$ due to the favourable propagation, which makes the direction any users' channels asymptotically orthogonal, i.e., $(\mathbf{H}^H\mathbf{H}/M) \rightarrow \mathbf{I}_N$, when $M \rightarrow \infty$, where $(\cdot)^H$ denotes the Hermitian transpose operator. This property makes linear receivers sufficient for mitigating interference between users (Björnson *et al.*, 2017). Nevertheless, numerical results will show that the performance of these receivers is far from that of the optimum detector, even for moderate load factors. In fact, for $\lambda = 1$, linear detection algorithms exhibit the lowest system performance.

Figure 1.5 shows the linear detection procedure, where the receiver first nullifies interference by multiplying the received symbols vector $\mathbf{r}$ by a weight matrix $\mathbf{W} \in \mathbb{C}^{N\times M}$. Then, the entries of the resultant vector, $\mathbf{z}$, are detected individually to obtain the estimated transmitted symbols

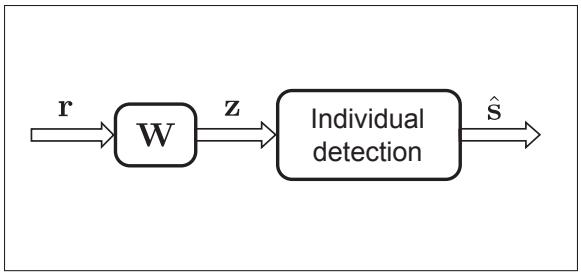

Figure 1.5 Linear detection procedure

vector, given by

$$\hat{\mathbf{s}} = \arg\min_{\mathbf{s}} \| \mathbf{z} - \mathbf{s} \|^2 . \tag{1.24}$$

Linear receivers include maximum ratio combining (MRC), zero-forcing (ZF), and minimum mean square error (MMSE), which are detailed below.

1.5.3.1 Maximum ratio combining

The MRC receiver, also known as matched filter (Chockalingam & Rajan, 2013), is a simple detector that treats the users' interference as noise. MRC mitigates the channel effects by the weighting matrix given by

$$\mathbf{W}_{MRC} = \mathbf{H}^H, \tag{1.25}$$

which is the Hermitian transpose of the channel matrix. Then, applying (1.25) to the received vector $\boldsymbol{r}$, we obtain

$$\begin{aligned} \mathbf{z}_{\text{MRC}} &= \mathbf{W}_{\text{MRC}}\mathbf{r} \\ &= \mathbf{W}_{\text{MRC}}(\mathbf{Hs} + \mathbf{n}) \\ &= \tilde{\mathbf{s}} + \mathbf{n}_{\text{MRC}}, \end{aligned} \tag{1.26}$$

where $\mathbf{n}_{\text{MRC}} = \mathbf{W}_{\text{MRC}}\mathbf{n}$ is a zero-mean colored Gaussian noise and $\tilde{\mathbf{s}} = \mathbf{W}_{\text{MRC}}\mathbf{Hs}$. Replacing $\mathbf{z}$ by $\mathbf{z}_{\text{MRC}}$ in (1.24), the estimated vector $\hat{\mathbf{s}}$ is obtained by the hard decision procedure. This operation

is expressed as

$$\hat{\mathbf{s}} = \mathbb{Q}(\mathbf{z}_{\text{MRC}}), \tag{1.27}$$

where $\mathbb{Q}(\cdot)$ denotes the element-wise quantization operation appropriate to the constellation in use. Finally, the complexity cost of the MRC detection is $O[MN]$.

1.5.3.2 Zero-Forcing

The ZF technique is a linear detector that mitigates the multi-user interference by the weight matrix given by

$$\mathbf{W}_{\text{ZF}} = (\mathbf{H}^H\mathbf{H})^{-1}\mathbf{H}^H, \tag{1.28}$$

which is the pseudo-inverse of the channel matrix $\mathbf{H}$. The nulling interference process is obtained by solving the following minimization problem (Chockalingam & Rajan, 2013):

$$\begin{aligned} \mathbf{z}_{\text{ZF}} &= \arg\min_{\mathbf{s}\in\mathbb{C}^N} \parallel \mathbf{r} - \mathbf{H}\mathbf{s} \parallel^2 \\ &= \mathbf{W}_{\text{ZF}}\mathbf{r} \\ &= \mathbf{W}_{\text{ZF}}(\mathbf{H}\mathbf{s} + \mathbf{n}) \\ &= \mathbf{s} + \mathbf{n}_{\text{ZF}}. \end{aligned} \tag{1.29}$$

where $\mathbf{n}_{\text{ZF}} = \mathbf{W}_{\text{ZF}}\mathbf{n}$ is a zero-mean colored Gaussian noise with a non-diagonal covariance matrix $\mathbf{K}_{\text{ZF}}$. Then the estimated symbols vector, $\hat{\mathbf{s}}$, is obtained as

$$\hat{\mathbf{s}} = \mathbb{Q}(\mathbf{z}_{\text{ZF}}). \tag{1.30}$$

The diversity gain achieved by the ZF detection is $M - N + 1$, and the complexity of the ZF detector is proportional to the pseudo-inverse of the $M \times N$ channel matrix $\mathbf{H}$, which is $O[N^3 + (3M + \frac{1}{2})N^2 + (M + \frac{1}{2})N]$. However, the ZF operation, in addition to nulling the interference, enhances the noise power $\mathbb{E}\{\parallel \mathbf{n}_{\text{ZF}} \parallel^2\}$, directly affecting the system's performance (Cho *et al.*, 2010).

1.5.3.3 Minimum Mean Square Error

The MMSE detector is a linear detection algorithm whose weight matrix is the matrix that minimizes the mean square error between the transmit vector and the estimated vector. Hence, the MMSE weigh matrix is obtained as (Chockalingam & Rajan, 2013)

$$\begin{aligned} \mathbf{W}_{\text{MMSE}} &= \arg\min_{\mathbf{W}} \mathbb{E}\left\{ \| \mathbf{s} - \mathbf{W}\mathbf{r} \|^2 \right\} \\ &= (\mathbf{H}^{\mathcal{H}}\mathbf{H} + \sigma_n^2\mathbf{I})^{-1}\mathbf{H}^{\mathcal{H}}. \end{aligned} \tag{1.31}$$

This expression maximizes the post-detection signal-to-interference plus noise ratio. The MMSE receiver requires knowledge of the noise variance of the received signal. Then, the resulting vector, after nulling the interference, is given by (Cho *et al.*, 2010)

$$\begin{aligned} \mathbf{z}_{\text{MMSE}} &= \arg\min_{\mathbf{s}\in\mathbb{C}^N} \| \mathbf{r} - \mathbf{H}\mathbf{s} \|^2 + \kappa \| \mathbf{s} \|^2 \\ &= \mathbf{W}_{\text{MMSE}}\mathbf{r} \\ &= \mathbf{W}_{\text{MMSE}}(\mathbf{H}\mathbf{s} + \mathbf{n}) \\ &= \tilde{\mathbf{s}} + \mathbf{n}_{\text{MMSE}}, \end{aligned} \tag{1.32}$$

where $\kappa > 0$. Applying hard decision to (1.32), the estimated signal vector is given by

$$\hat{\mathbf{s}} = \mathbb{Q}(\mathbf{z}_{\text{MMSE}}). \tag{1.33}$$

The diversity gain of the MMSE receiver is $M - N + 1$ for high rates (Mehana & Nosratinia, 2010). The complexity of this technique is $O[N^3 + (6M + \frac{3}{2})N^2 + (M + \frac{1}{2})N]$, which is quite similar to the ZF complexity.

1.5.4 Non-linear detection

In contrast to linear detection, non-linear detection algorithms exhibit better performance at the expense of high complexity. Classical non-linear MU-MIMO receivers are the ML, sphere decoding (SD), and ordered successive interference cancellation (OSIC).

ML is the optimal vector-symbol detector that achieves the optimum performance at maximum a posteriori (MAP) detection. However, its complexity increases exponentially with the number of UEs $O[\mathcal{M}]$, as described earlier. This condition makes its implementation unfeasible for large MU-MIMO systems. However, the ML algorithm is feasible for a small number of UEs (Chockalingam & Rajan, 2013).

The SD algorithm estimates the transmitted symbols vector by searching inside a sphere radius parameter rather than all possible transmitted vectors. The SD method adjusts the radius until obtaining the vector-symbol solution within the sphere. Thus, by choosing a large enough radius, the SD performance approaches that of the ML detector (Cho *et al.*, 2010). However, the size of the radius parameter is inversely proportional to the noise variance. Thus, for low SNRs, the radius search becomes high, and it exhibits exponential complexity proportional to the total number of UEs, which makes the SD unfeasible for large MU-MIMO systems (Chockalingam & Rajan, 2013).

The OSIC detector was proposed to improve the linear detection without significaltly increasing the complexity (Foschini, 1996). The OSIC is a multistage receiver composed of a bank of ZF or MMSE receivers. The main steps of the OSIC detection are as follows: 1) the interference cancellation step, which is the interference subtraction from the already detected symbols; 2) the interference nulling step, where the interference from the yet-to-be-detected symbols can be nulled out by the Gram–Schmidt orthogonalization process applied to the column vectors of the channel matrix; 3) the optimal ordering step, which orders the symbols to be detected according to their SNRs (Loyka & Gagnon, 2004). The diversity gain for the ith UE can reach a diversity gain of $M - N + i$ if the previously-detected UEs' symbols are detected correctly (Cho *et al.*, 2010). The complexity of OSIC is given by $O\left[\frac{N^4}{4} + MN^3 + \left(\frac{5M}{2} + \frac{1}{2}\log_2 N!\right)N^2 + \left(\frac{9M}{2} + \frac{1}{2}\log_2 N!\right)N\right]$. Finally, it is well known that OSIC outperforms linear receivers. However, its performance is far from optimum, and its complexity does not scale well for large MU-MIMO systems (Chockalingam & Rajan, 2013).

1.5.5 Complexity comparison

We compare the complexity of linear and non-linear receivers in terms of FLOPs versus the number of UEs in Figure 1.6. As expected, MRC exhibits the lowest complexity, while the complexity of ZF and MMSE are quite similar. The complexity of OSIC is one order of magnitude greater than that of the ZF and MMSE receivers. On the other hand, we do not plot the complexity of ML and SD algorithms because of their exponential complexity; e.g., for $N = 128$, the complexity of ML is 7.5×10^{81} FLOPs.

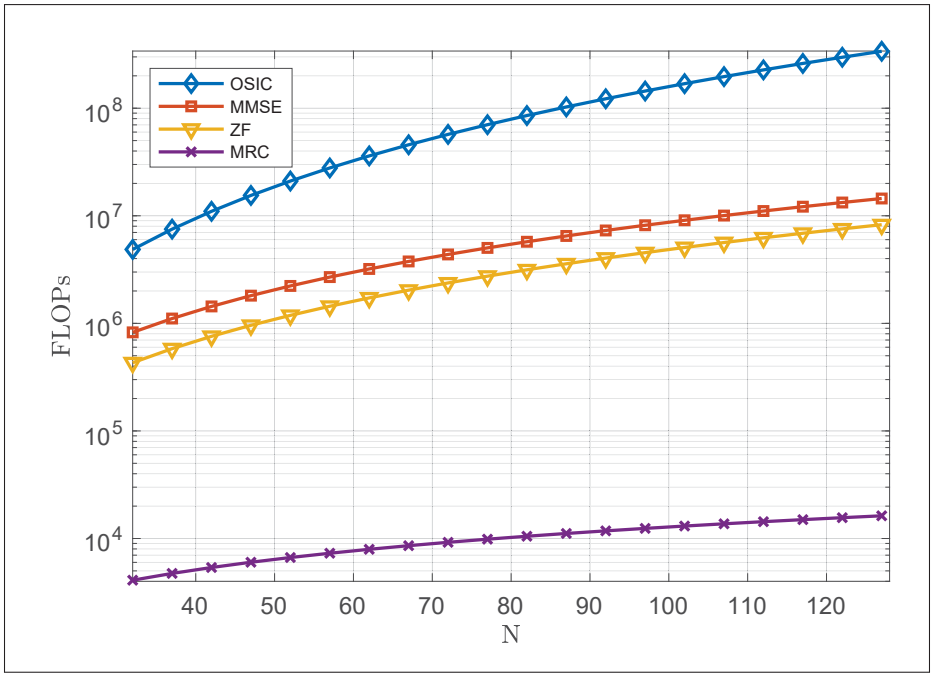

Figure 1.6 Complexity of OSIC, MMSE, ZF, and MRC receivers for large MU-MIMO systems with $M = 128$

Since non-linear receivers' complexity is extremely high, especially for large MU-MIMO systems, we only evaluate the performance of MRC, ZF, and MMSE receivers.

1.5.6 Numerical results of linear receivers' performance

In this chapter, we will use the BER to evaluate the receivers' performance. We consider a large MU-MIMO system with $M = 128$ antennas at the BS and $N = \{32, 120, 128\}$ UEs that achieve $\lambda = \{0.25, 0.9, 1\}$ load factors, respectively. We assume that each user transmits 4-QAM symbols sequence over the channel described in (1.10) for the distributed antenna layout. Thus, the transmit and receive correlation matrices are $\mathbf{\Sigma}(\rho_t = 0.5)$ and $\mathbf{\Psi} = \mathbf{I}$, respectively. Then, the performance results are expressed in terms of BER versus E_b/N_0.

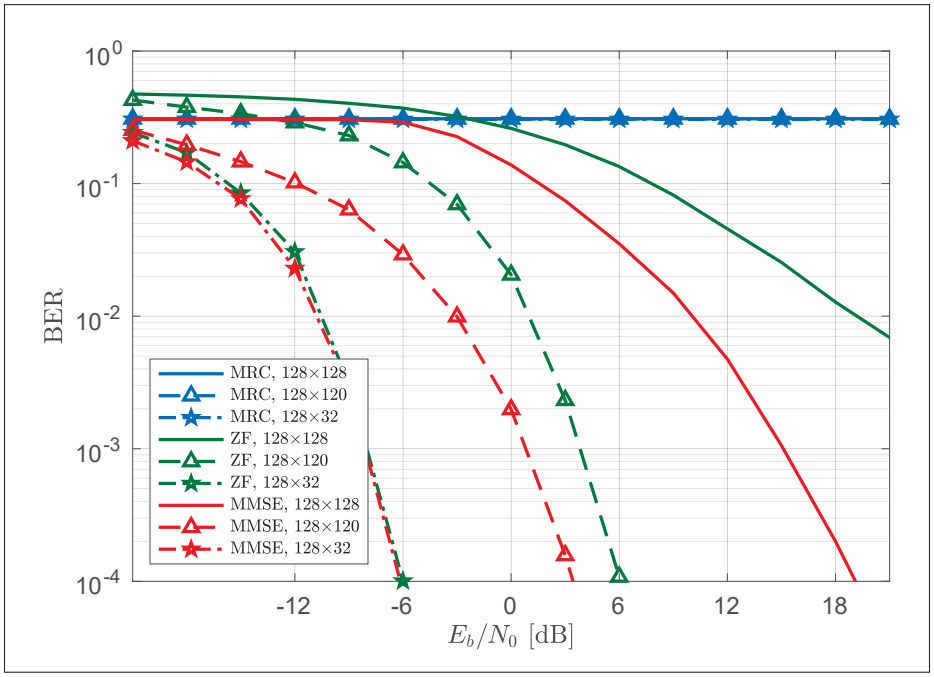

Figure 1.7 BER vs E_b/N_0 performance of MMSE, ZF, and MRC receivers for large MU-MIMO with $\mathbf{\Sigma}(\rho_t = 0.5)$, $\mathbf{\Psi} = \mathbf{I}$, $M = 128$, $N = \{32, 120, 128\}$, and 4-QAM modulation

Figure 1.7 shows the BER performance of the MRC, ZF, and MMSE receivers. We observe that the MRC receiver's performance is severely degraded, even for $\lambda = 0.25$, where favourable propagation conditions are expected. Moreover, the performance of the ZF receiver is attractive for low and medium load factors, while it experiences severe degradation for full load factors.

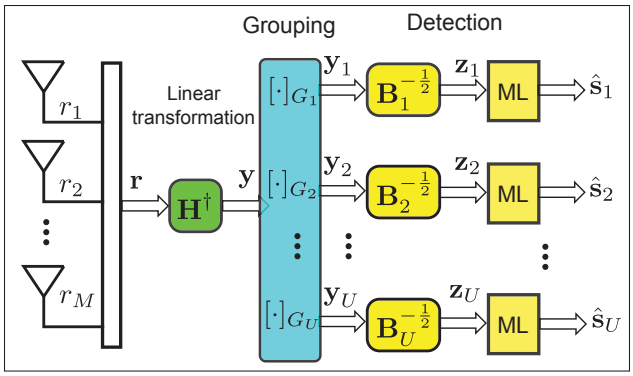

Figure 1.8 GD-ML receiver scheme
Adapted from Maza et al. (2020, p. 45655)

Furthermore, the MMSE detector achieves better performance than the MRC and ZF receivers for all considered scenarios. Nonetheless, like the ZF receiver, the MMSE performance experiences a severely degradation for $\lambda = 1$.

1.6 GD-ML technique

In the previous section, we showed that linear receivers exhibit poor performances for moderate and full-load factors in large MU-MIMO systems; however, their complexity is quite attractive. For that reason, we focus our interest on studying the GD-ML receiver to enhance the performance of low-complexity linear receivers. This receiver improves the ZF receiver's performance by adding a negligible extra complexity. Thus, this section presents key concepts of the group detection technique: the general structure, complexity analysis, and numerical results.

1.6.1 Receiver structure

In general, the group detection receiver consists of three steps (Cal-Braz & Sampaio-Neto, 2014; Maza *et al.*, 2020): 1) linear transformation of the received vector, 2) division of the result into groups, and 3) detection within each group, as shown in Figure 1.8.

1.6.1.1 Linear transformation

At the receiver, the transmitted symbols vector is multiplied by the channel matrix, which makes the vector division difficult. Thus, a linear transformation is performed to isolate the transmitted symbols alone by removing the channel matrix, thus facilitating group formation. The linear transformation process is applied by the pseudo-inverse of the channel matrix, expressed as

$$\mathbf{H}^{\dagger} = (\mathbf{H}^{H}\mathbf{H})^{-1}\mathbf{H}^{H}, \tag{1.34}$$

where $\mathbf{H}^{\dagger}\mathbf{H} = \mathbf{I}$. It is noted that the linear transformation matrix is equivalent to the weighting matrix of the ZF detection given in (1.28). Finally, the application of the linear transformation matrix to (1.15) yields the following resultant vector (Maza *et al.*, 2020)

$$\begin{aligned} \mathbf{y} &= \mathbf{H}^{\dagger}\mathbf{r} \\ &= \mathbf{H}^{\dagger}[\mathbf{H}\mathbf{s} + \mathbf{n}] \\ &= \mathbf{s} + \mathbf{v}, \end{aligned} \tag{1.35}$$

where $\mathbf{v} = \mathbf{H}^{\dagger}\mathbf{n}$ is a zero-mean colored Gaussian noise with the following covariance matrix (Maza *et al.*, 2020)

$$\begin{aligned} \mathbf{K} &= \mathbf{H}^{\dagger}(\mathbf{H}^{\dagger})^{H} \\ &= (\mathbf{H}^{H}\mathbf{H})^{-1}. \end{aligned} \tag{1.36}$$

We emphasize that the covariance matrix is non-diagonal due to the correlated channel model given in (1.9).

1.6.1.2 Grouping

In this subsection, we present the group formation process, in which the entire set of N UEs is separated into U groups, after the linear transformation. Each group contains N_u UEs, according

to the following grouping configuration

$$\mathcal{G}(U, N_1, \cdots, N_U) = \{G_1, \cdots, G_U\}, \tag{1.37}$$

where

$$G_u = \{k_{1,u}, \cdots, k_{N_u,u}\}, \tag{1.38}$$

represents a set of position indexes of the UEs that belongs the uth group, $k_{i,u} \in \{1, \cdots, N\}$, $i = 1, \cdots, N_u$, and $u = 1, \cdots, U$. Let $\mathbf{y}_u$ denote as the uth group vector given by (Maza *et al.*, 2020)

$$\begin{aligned} \mathbf{y}_u &= [\mathbf{y}]_{G_u} \\ &= \mathbf{s}_u + \mathbf{v}_u; \quad u = 1, 2, \ldots, U, \end{aligned} \tag{1.39}$$

where $[\cdot]_{G_u}$ returns a sub-vector with N_u elements of $\mathbf{y}$ in (1.35), such that $\mathbf{y}_u = [y_{k_{1,u}}, \cdots, y_{k_{N_u,u}}]^T$, where $y_{k_{i,u}}$ is the ith entry of the uth group vector. Moreover, $\mathbf{s}_u = [s_{k_{1,u}}, \cdots, s_{k_{N_u,u}}]^T$ is the transmitted signals vector and $\mathbf{v}_u = [v_{k_{1,u}}, \cdots, v_{k_{N_u,u}}]^T$ is the zero-mean uth group's colored noise vector with $N_u \times N_u$ covariance matrix expressed as (Maza *et al.*, 2020)

$$\mathbf{K}_u = (\mathbf{H}_u^H \mathbf{H}_u)^{-1}, \tag{1.40}$$

where $\mathbf{H}_u$ is the uth group channel matrix of size $M \times N_u$ given by (Maza *et al.*, 2020)

$$\begin{aligned} \mathbf{H}_u &= \mathbf{\Psi}^{\frac{1}{2}} \mathbf{A}_u \mathbf{\Sigma}_u^{\frac{1}{2}} \\ &= [\mathbf{h}_{k_{1,u}}, \cdots, \mathbf{h}_{k_{N_u,u}}], \end{aligned} \tag{1.41}$$

where $\mathbf{\Psi}$ is the $M \times M$ receive correlation matrix, $\mathbf{A}_u$ is the $M \times N_u$ i.i.d. Rayleigh-fading, and $\mathbf{\Sigma}_u$ is the $N_u \times N_u$ correlation matrix of the users pertaining to the uth group. Finally, $\mathbf{h}_{k_{i,u}}$ is the channel vector of the ith user in the uth group. In (1.41), we observe that $\mathbf{\Psi}$ is constant for all groups; hence, $\mathbf{\Psi}$ does not influence the group formation and the BER performance (Maza *et al.*, 2020).

1.6.1.3 Detection at each group

The estimation of the transmitted group symbols vector $\boldsymbol{s}_u$ through ML detection is considered since N_u is significantly lower than N, which greatly lowers the complexity cost. The ML algorithm is optimum for white noise whereas the noise in (1.39) is colored. Thus, we first whiten the noise and then proceed with the ML process. Let us define $\mathbf{B}_u$ as the whitening matrix given by

$$\begin{aligned} \mathbf{B}_u &= \mathbf{K}_u^{-\frac{1}{2}} \\ &= (\mathbf{H}_u^H \mathbf{H}_u)^{\frac{1}{2}}, \end{aligned} \tag{1.42}$$

where $\mathbf{K}_u^{-\frac{1}{2}} \mathbf{K}_u^{-\frac{1}{2}} = \mathbf{K}_u^{-1}$ and $\mathbf{B}_u^H = \mathbf{B}_u$. Moreover, let $\mathbf{B}^2$ define as the squared whitening matrix expressed as

$$\begin{aligned} \mathbf{B}_u^2 &= \mathbf{B}_u^H \mathbf{B}_u \\ &= \mathbf{H}_u^H \mathbf{H}_u, \end{aligned} \tag{1.43}$$

which will be useful for further analysis in Chapter 3. Then, $\mathbf{B}_u$ is applied to (1.39) to whiten the colored noise $\mathbf{v}_u$. Finally, the resulting vector $\mathbf{z}_u = [z_{u,1}, \cdots, z_{u_{N_u}}]$ is expressed as (Maza *et al.*, 2020)

$$\begin{aligned} \mathbf{z}_u &= \mathbf{B}_u \mathbf{y}_u \\ &= \mathbf{B}_u (\mathbf{s}_u + \mathbf{v}_u) \\ &= \mathbf{B}_u \mathbf{s}_u + \tilde{\mathbf{n}}_u, \end{aligned} \tag{1.44}$$

where $\tilde{\mathbf{n}}_u = \mathbf{B}_u \mathbf{v}_u$ is a zero-mean white Gaussian noise vector with covariance matrix

$$\begin{aligned} \mathbf{K}_{\tilde{\mathbf{u}}_u} &= \mathbf{B}_u \mathbf{K}_u \mathbf{B}_u^H \\ &= \mathbf{K}_u^{-\frac{1}{2}} \mathbf{K}_u^{\frac{1}{2}} \mathbf{K}_u^{\frac{1}{2}} \mathbf{K}_u^{-\frac{1}{2}} \\ &= \mathbf{I}_{N_u}. \end{aligned} \tag{1.45}$$

Then, the estimation of the transmitted group symbols vector can be expressed as (Maza *et al.*, 2020)

$$\hat{\mathbf{s}}_u = \arg \min_{\mathbf{s}_u \in \mathcal{S}_u} \left[\| \mathbf{B}_u \mathbf{s}_u - \mathbf{z}_u \|^2 \right], \tag{1.46}$$

where $\mathcal{S}_u$ is the set of signal constellation points with $\mathcal{M}_u = \mathcal{A}^{N_u}$ elements. Note that $\mathcal{M}_u$ is much smaller than the size of the global optimum receiver symbols constellation set (Maza *et al.*, 2020), i.e., $\mathcal{M}_u \ll \mathcal{M}$.

1.6.2 GD-ML complexity efficiency analysis

Let C_{GD} denote the complexity of the GD-ML receiver, which refers to the FLOPs required to estimate the transmitted group symbols vector, given as

$$\begin{aligned} C_{GD} &= C_{LT} + C_{GR} + C_{ML} \\ &= \mathcal{O}\left[N^3 + \left(3M + \frac{1}{2}\right) N^2 + \left(M + \frac{3}{2}\right) N \right. \\ &\quad \left. + \mathcal{M}_u \left(2N_u^2 + 2N_u - 1\right) \right], \end{aligned} \tag{1.47}$$

where C_{LT}, C_{GR}, and C_{ML} are the complexities of linear projection, grouping, and ML stages, respectively.

First, we present the complexity results of the ZF, MMSE, and GD-ML receivers with group size $N_u = \{2, 3, 4, 5, 6, 7, 8\}$, which are exhibited in Figure 1.9. We notice that the complexity of the GD-ML is dominated by the linear transformation complexity C_{LT}, which involves the channel matrix inversion. Furthermore, a negligible complexity proportional to the group size is added by the ML detection and grouping stages, which we denote as $C_{EX} = C_{GR} + C_{ML}$; hence, $C_{GD} \gg C_{EX}$. We also observe that the gap between the complexity of the GD-ML and the linear receivers is inversely proportional to the number of UEs (Maza *et al.*, 2020). We highlight that C_{LT} equals the ZF receiver's complexity and we also consider C_{LT} similar to the complexity of the MMSE receiver.

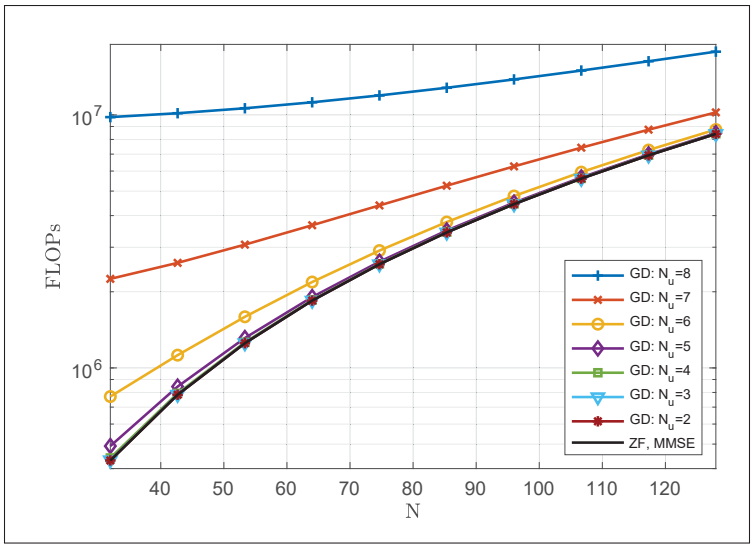

Figure 1.9 Complexity comparison of ZF, MMSE, and GD-ML receiver with $N_u = \{2, 3, 4, 5, 6, 7, 8\}$ for large MU-MIMO with $M = N$. 4-QAM modulation

Second, we evaluate the complexity efficiency of GD-ML for full-load large MU-MIMO systems by determining the percentage of extra complexity that GD-ML exceeds the ZF and MMSE receivers' complexity, which we denote as.

$$C_{EX}\% = (C_{GR} + C_{ML}) \times 100\%. \tag{1.48}$$

Then, we define a threshold, $Th = 1\%$, which is a percentage of additional complexity over linear receivers' complexity. We consider this parameter a complexity criterion for choosing the appropriate group size for a given N. Figure 1.10 shows the $C_{EX}\%$ versus N_u that the GD-ML with $N_u = \{2, 3, 4, 5, 6, 7, 8\}$ requires for different $N = \{8, 16, 32, 64, 128\}$ and $M = N$. We observe that $C_{EX}\%$ decreases as the number of UEs increases, allowing an increment in group size without exceeding the given threshold; e.g., a GD-ML with group size $N_u = 5$ requires an extra complexity percentage of 0.7% for $N = 128$ which does not exceed the threshold criterion, while for $N = 32$ it requires 45.5%. Based on these results, we conclude that the GD-ML receiver is more suitable for large MU-MIMO systems.

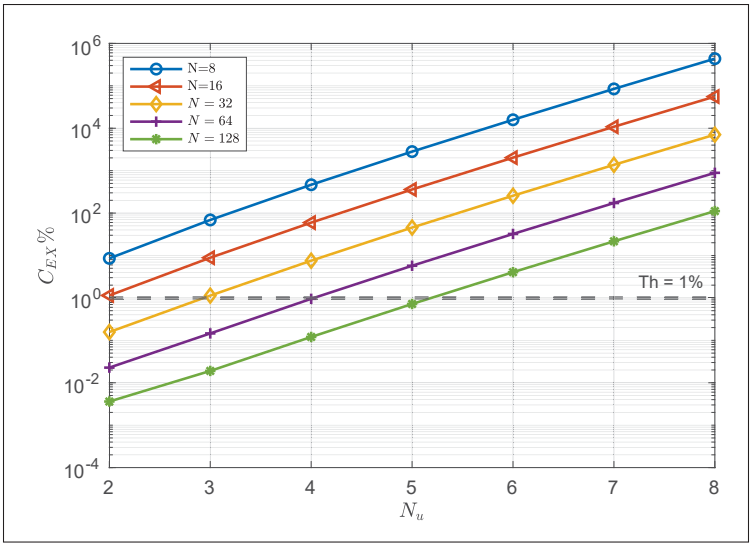

Figure 1.10 C_{EX}% vs. N_u of GD-ML receiver with $N_u = \{2, 3, 4, 5, 6, 7, 8\}$ for $N = \{8, 16, 32, 64, 128\}$ and $M = N$

1.6.3 GD-ML numerical results performance

The GD-ML receiver's performance was simulated in Matlab as described in Algorithm 1.1. We also assume that the UEs transmit 4-QAM symbols over the correlated channel with a distributed antenna configuration, with $\mathbf{\Psi} = \mathbf{I}_M$ and $\mathbf{\Sigma}(\rho_t = 0.5)$. The performance is evaluated in terms of BER versus E_b/N_0, which are presented as follows:

- *Group size performance evaluation:* Without loss of generality, we consider $N = 5$ UEs and $M = 5$ antennas at the BS instead of large MU-MIMO systems. Figure 1.11 shows the BER performance for $N_u = \{1, 2, 3, 4, 5\}$. The results of the GD-ML receiver are compared to that of the ZF and ML receivers. It is shown that the GD-ML receiver with group size $N_u = 1$ yields the same performance as the ZF receiver. In contrast, when the group size is $N_u = 5$, the GD-ML receiver achieves the ML receiver's performance, which implies that the GD-ML's performance is proportional to the group size N_u.
- *Performance for group size with threshold complexity:* Figure 1.12 shows the BER performance of the GD-ML receivers with group sizes that meet the 1% extra complexity criteria for $N = 128$ and $M = 128$, i.e., $N_u \leq 5$. These results are compared with the ZF and MMSE

Algorithm 1.1 Algorithm of GD-ML Receiver

Input: $\mathbf{r}$, $\mathbf{H}$, U, N_u, $\{G_1, \cdots, G_U\}$, $G_u = \{k_{1,u}, \cdots, k_{N_u,u}\}$
Output: $\hat{\mathbf{s}}_1, \hat{\mathbf{s}}_2, \cdots, \hat{\mathbf{s}}_U$

$\mathbf{H}^{\dagger} \leftarrow (\mathbf{H}^H\mathbf{H})^{-1}\mathbf{H}^H$;
$\mathbf{y} \leftarrow \mathbf{H}^{\dagger}\mathbf{r}$;
for *all references* $G_u = \{k_{1,u}, \cdots, k_{N_u,u}\}$ **do**
    $\mathbf{y}_u \leftarrow [\mathbf{y}]_{G_u}$;
    $\mathbf{K}_u \leftarrow (\mathbf{H}_u^H\mathbf{H}_u)^{-1}$;
    $\mathbf{B}_u \leftarrow \mathbf{K}_u^{-\frac{1}{2}}$;
    $\mathbf{z}_u \leftarrow \mathbf{B}_u\mathbf{y}_u$;
    $\hat{\mathbf{s}}_u \leftarrow \arg\min_{\mathbf{s}_u \in \mathcal{S}_u} \left[\| \mathbf{B}_u\mathbf{s}_u - \mathbf{z}_u \|^2\right]$;
end for

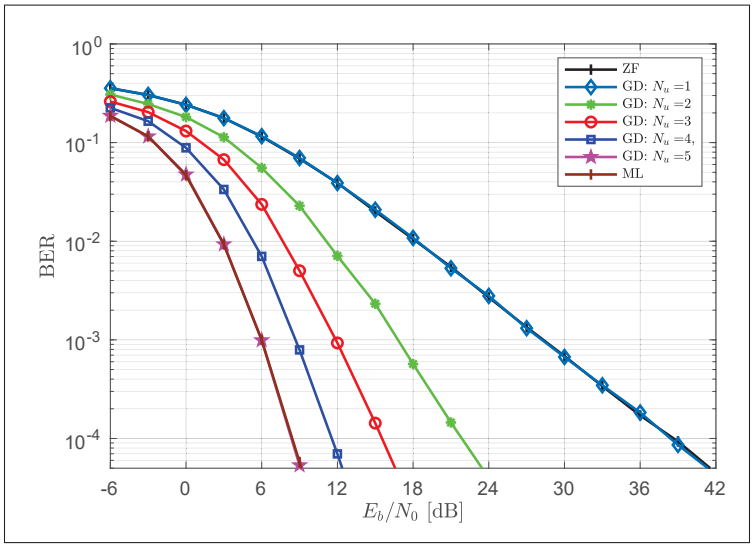

Figure 1.11 Group size performance evaluation for GD-ML receiver and $N = 5$ and $M = 5$, and $\rho_t = 0.5$

receivers' performance. We observe that the GD-ML receiver with $N_u \geq 2$ and $N_u \geq 3$ outperforms the ZF and MMSE receivers, respectively. Hence, for BER $= 10^{-4}$, the GD-ML with group size $N_u = 5$ yields an E_b/N_o gap of 28dB compered to the ZF and a gap of 8dB compered to the MMSE receiver.

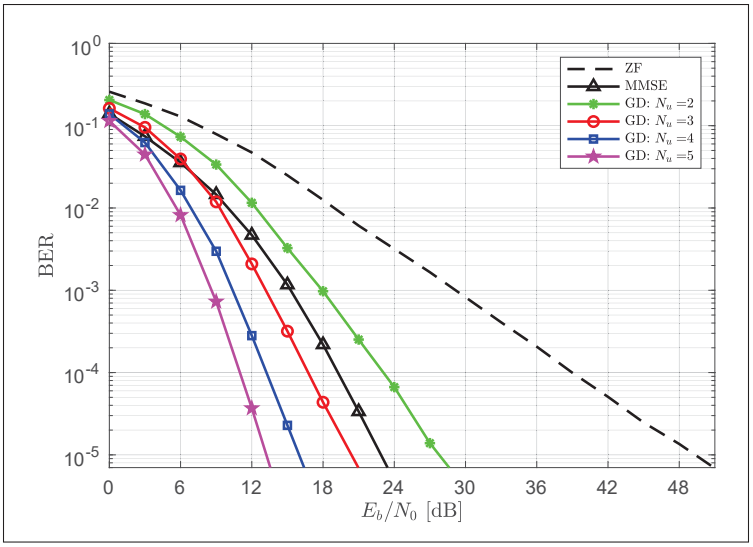

Figure 1.12 BER performance versus E_b/N_o of ZF, MMSE, and GD-ML with $N_u = \{2,3,4,5\}$. $N = 128$, $M = 128$, and $\rho_t = 0.5$

CHAPTER 2

LITERATURE REVIEW AND RELATED WORKS

2.1 Overview

The GD-ML technique was introduced by Varanasi (1995) for multi-user detection in code-division multiple-access (CDMA) channels. Since then, GD-ML has been studied extensively for orthogonal frequency-division multiplexing (OFDM) and single-carrier systems (Bayramoglu, Karjalainen & Juntti, 2013; Maza, Sampaio-Neto & Medina, 2012), as well as for MIMO technologies.

In the preceding chapter, we introduced the GD-ML receiver, which comprises the ZF linear projection, fixed grouping strategy, and ML detection stages. This chapter shows the related research on the GD-ML receiver divided into two sections. The first section summarizes the proposed receiver structures, focusing on the benefits of the structure adopted in this thesis. The second section covers the relevant works related to the GD-ML performance analysis, highlighting their limitations and potential opportunities for further research.

2.2 GD-ML structure

The study of GD-ML structure comprises four main stages, illustrated in Figure 2.1. These stages include linear projection methods, grouping strategies, detection methods into each group, and post-detection.

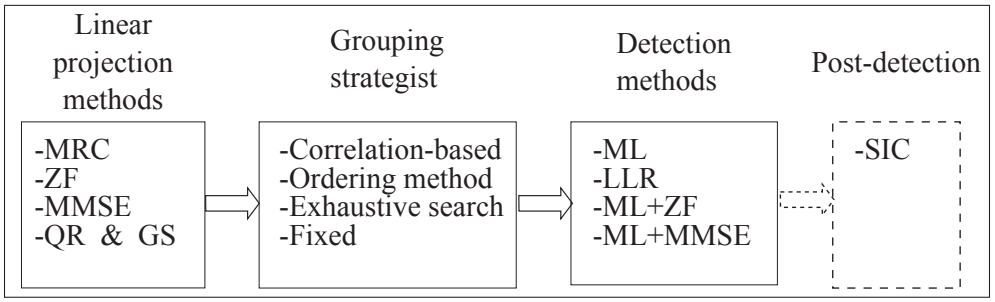

Figure 2.1 Scheme of GD-ML structure study

2.2.1 Linear projection methods

The linear projection is a matrix operation process that is applied to cancel the channel effects from the UE and prepare the received symbols vector for group formation. The common linear projection algorithms are MRC, ZF, MMSE, and the QR decomposition combined with the Grand-Smith (GS) orthogonalization that we describe as follows:

- *MRC:* the authors in (Krause, Taylor & Martin, 2011) suggested using MRC as a linear projector for overloaded MIMO systems. This involves using the Hermitian transpose of the channel matrix on the received symbols vector, which is ideal for low load factor large MIMO systems with favorable propagation conditions. Despite its low complexity advantage, we showed that MRC exhibit poor performance even for medium and low load factors, which means that it does not mitigate the channel effects efficiently.
- *ZF:* numerous studies have proposed the use of ZF linear projection, which involves applying the pseudo-inverse channel matrix operation to the received symbols vector (Li, Huang, Lozano & Foschini, 2000; Sfar & Letaief, 2003; Cal-Braz & Sampaio-Neto, 2014). This procedure effectively eliminates channel effects, making the symbol vector ready to be divided into groups. However, a major drawback is the amplification of the noise power, leading to poor performance in low SNR situations. The complexity of the matrix inversion, and consequently this method increases with the increase in the number of UEs, which could create a disadvantageous breakpoint. However, several efficient matrix inversion algorithms have been introduced, making this linear projection method an attractive option for large MU-MIMO.
- *MMSE:* research on MMSE as a linear projection method for conventional MIMO was presented in (Elkhazin, Plataniotis & Pasupathy, 2006; Choi, Shim, Singer & Cho, 2010; Yang, Hu & Zhang, 2007; Moon, Jeong, Lee & Lee, 2010). The authors in (Choi *et al.*, 2013; Nguyen *et al.*, 2018a; Nguyen, Le, Ngo & Nguyen, 2018b) studied its use in uplink massive MIMO, while Liu, Yang, Sun, Zhang & Qian (2022) explored its application for downlink massive MIMO. In contrast to ZF, the MMSE linear projector takes into account the noise effects, thus achieving better performance at low SNRs while its complexity is slightly higher.

However, this linear projector can not convert the channel matrix into an identity matrix, thus challenging the grouping process and performance analysis.

- *QR & GS:* the authors in (Choi, Negi & Cioffi, 2000) have implemented a linear projection to separate the received symbols vector into two groups using the QR decomposition and Gram–Schmidt (GS) orthogonalization procedures. This method's main advantage lies in its ability to form independent groups, which theoretically mitigates inter-group interference. However, this method is unsuitable for multiple groups due to the complexity introduced by the orthogonalization process.

In this thesis, we opted for the ZF linear projection method because it effectively mitigated the channel effects. This facilitates the groups' formation since the symbols vector stays intact due to the channel matrix's identity conversion. Additionally, it simplifies the performance analysis, which is the main contribution of this thesis.

2.2.2 Grouping strategies

Grouping strategies have been developed to maximize the group or system performance while minimizing the computational cost. The two most notable methods found in the literature are correlation-based and ordering-based strategies, which we discuss in detail below.

- *Correlation-based:* this grouping method was proposed in (Li *et al.*, 2000; Elkhazin *et al.*, 2006). This method involves analyzing the correlation between the UEs using the correlation channel matrix to group the least correlated UEs together.
- *Ordering-based:* according to (Choi *et al.*, 2000; Sfar & Letaief, 2003; Sfar, Dai & Letaief, 2005; Cal-Braz & Sampaio-Neto, 2014; Krause *et al.*, 2011; Moon *et al.*, 2010; Choi *et al.*, 2013), the ordering-based method involves arranging the UEs based on their channel power, SNR, and SINR. This approach is particularly useful for GD-ML receivers using SIC.
- Several alternative grouping methods, such as exhaustive search and fixing strategies, have been explored for performance and complexity comparisons (Bayramoglu *et al.*, 2013). Exhaustive search algorithms consider all possible combinations, which is also known as brute force. However, this approach is not the most efficient due to its high computational

cost. On the other hand, the fixing grouping method permanently assigns members to each group, which offers the advantage of low computational cost.

In this research work, we chose the fixing grouping method because it does not directly influence the performance analysis result.

2.2.3 Detection methods for each group

The GD-ML technique offers the significant benefit of enabling optimal detection within each group, thanks to the small number of UE symbols that need to be estimated. Thus, the ML detector usage in each group for conventional MIMO has been studied in (Li *et al.*, 2000; Sfar & Letaief, 2003; Choi *et al.*, 2000, 2010; Bottomley & Wang, 2010; Moon *et al.*, 2010; Krause *et al.*, 2011) and for massive MIMO systems was proposed by (Nguyen *et al.*, 2018a,b). Additionally, the log-likelihood-ratio algorithm, which maximizes the posterior probability for coded conventional MIMO systems, was proposed by (Elkhazin *et al.*, 2006; Yang *et al.*, 2007), while (Choi *et al.*, 2013) explored this technique for massive MIMO.

Furthermore, the use of a combination of ML and ZF detectors was introduced by (Choi *et al.*, 2000), while (Choi *et al.*, 2010) presented the alternative of combining ML with MMSE. These approaches were proposed to reduce the complexity of the ML algorithm.

Since the main objective of this thesis is the derivation of the performance analysis, we considered using only an ML detection for each group and discarding the combination with other receivers to simplify the performance analysis.

2.2.4 Post-detection

Many studies on GD-ML receivers have incorporated a post-detection process to improve their performance. Many approaches (Li *et al.*, 2000; Sfar & Letaief, 2003; Krause *et al.*, 2011) involve employing the successive interference cancellation (SIC) for conventional MIMO systems, while

for massive MIMO ware studied by (Nguyen *et al.*, 2018b,a). SIC mitigates the interference caused by previously detected symbol groups.

This technique yields a high complexity cost for a large number of groups, which makes it unsuitable for large MIMO environments; thereby, we did not consider its usage in this thesis.

2.3 GD-ML performance analysis for MIMO systems

The group detection technique has been extensively researched for MIMO systems, exploring various receiver structures and grouping strategies. However, most of the available works are simulations (Li *et al.*, 2000; Bottomley & Wang, 2010; Choi *et al.*, 2010; Moon *et al.*, 2010; Cal-Braz & Sampaio-Neto, 2014). To the best of the authors' knowledge, only two studies have considered the performance analysis of GD-ML receivers.

The first study proposed by (Choi *et al.*, 2000) investigated the upper bound performance for all symbols pertaining to the same group, named block error probability, which is equivalent to the VEP (Vector-symbol error probability) defined in the previous chapter. The results have shown that the GD-ML achieves a diversity order proportional to the group size. However, this work is limited to conventional MIMO systems with co-located antennas at the BS. It also assumes an i.i.d. Rayleigh channel, simplifying the distribution of the random variables used to derive the receiver's performance.

The second research made by (Elkhazin *et al.*, 2006) provided the union bound of VEP for uncoded MIMO systems based on the maximum a-posterior probability (MAP) process and soft-input soft-output (SISO). However, in addition to the limitations of the first research paper, this article presents the receiver's performance as a non-closed mathematical expression that contains summations and functions to be solved.

The aforementioned limitations present research opportunities for deriving a closed-form expression for the GD-ML receiver performance in large MU-MIMO systems with correlated channels and distributed antennas, which is one of the main contributions of this thesis.

CHAPTER 3

GD-ML PERFORMANCE ANALYSIS

3.1 Overview

In this chapter, we derive a closed-form expression for the average PE (probability of error) for the uth group, considered the GD-ML receiver's structure, which includes linear projection, grouping, and ML detection into each group. Considering that the linear projection has the same influence on all groups and assuming an ideal grouping strategy, the group performance is subject to the ML detection stage. The ML detection technique detects all symbols jointly; as a consequence, it is natural to consider the group VER to evaluate its performance (Talwar & Paulraj, 1997).

The rest of this chapter is organized as follows: In Section 3.2, we define the group VER of the GD-ML receiver, while in Section 3.3, we derive its upper bound. Section 3.4 presents the distribution of minimum Euclidean distance, which is a key factor in deriving the average group VER. The closed-from expression of the average group VER is derived in Section 3.5. Finally, in Section 3.6, numerical results are presented to verify the derived analytical expression.

3.2 Group VER

Let PE_u denote the VER of the uth group, which is defined as the probability that, after the whitening process, at least one symbol of the estimated vector is not equal to the corresponding symbol in the transmitted vector, expressed as (Maza *et al.*, 2020)

$$PE_u \triangleq \Pr\{\hat{\mathbf{s}}_u \neq \mathbf{s}_u | \mathbf{B}_u\}. \tag{3.1}$$

Let us define the pair-wise error probability as the probability of detecting $\mathbf{s}_{u,j}$ when $\mathbf{s}_u = \mathbf{s}_{u,i}$ is the transmitted symbols vector, given as (Maza *et al.*, 2020)

$$\Pr\{\mathbf{s}_{u,i} \longrightarrow \mathbf{s}_{u,j}|\mathbf{B}_u\} = Q\left(\sqrt{\frac{d_{u,ij}^2}{2}\gamma}\right); i, j = 1, \cdots, \mathcal{M}_u, \quad \forall i \neq j, \tag{3.2}$$

where $\gamma = 1/N_o$ is the SNR, and $d_{u,ij}^2$ is the squared Euclidean distance between $\mathbf{s}_{u,i}$ and $\mathbf{s}_{u,j}$ expressed as (Maza *et al.*, 2020)

$$\begin{aligned} d_{u,ij}^2 &= \| \mathbf{B}_u(\mathbf{s}_{u,i} - \mathbf{s}_{u,j}) \|^2 \\ &= \mathbf{e}_{u,ij}^H \mathbf{B}_u^H \mathbf{B}_u \mathbf{e}_{u,ij} \\ &= \mathbf{e}_{u,ij}^H \mathbf{B}_u^2 \mathbf{e}_{u,ij}, \end{aligned} \tag{3.3}$$

where $\mathbf{e}_{u,ij} = \mathbf{s}_{u,i} - \mathbf{s}_{u,j}$, and $\mathbf{B}_u^2$ is the squared group whitening matrix defined in (1.43).

The event PE_u given in (3.1) can be derived by the law of total probability. For a set of all $\mathcal{M}_u$ possible equiprobable symbol vectors, $\mathbf{s}_{u,i}$, PE_u is given by (Maza *et al.*, 2020; Talwar & Paulraj, 1997)

$$\begin{aligned} PE_u &= \sum_{i=1}^{\mathcal{M}_u} \left[PE_u|\mathbf{s}_u = \mathbf{s}_{u,i}, \mathbf{B}_u\right] \Pr(\mathbf{s}_u = \mathbf{s}_{u,i}) \\ &= \frac{1}{\mathcal{M}_u} \sum_{i=1}^{\mathcal{M}_u} \left[PE_u|\mathbf{s}_u = \mathbf{s}_{u,i}, \mathbf{B}_u\right], \end{aligned} \tag{3.4}$$

where the conditional PE, $\left[PE_u|\mathbf{s}_u = \mathbf{s}_{u,i}, \mathbf{B}_u\right]$, can be bounded by the sum of the pair-wise error probabilities, given in (3.2), as (Maza *et al.*, 2020)

$$\left[PE_u|\mathbf{s}_u = \mathbf{s}_{u,i}, \mathbf{B}_u\right] \leq \sum_{\substack{j=1, \\ j \neq i}}^{\mathcal{M}_u} Q\left(\sqrt{\frac{d_{u,ij}^2}{2}\gamma}\right). \tag{3.5}$$

Substituting (3.5) in (3.4), we obtain

$$PE_u \leq \frac{1}{\mathcal{M}_u} \sum_{i=1}^{\mathcal{M}_u} \sum_{\substack{j=1, \\ j \neq i}}^{\mathcal{M}_u} Q\left(\sqrt{\frac{d_{u,ij}^2}{2}\gamma}\right). \tag{3.6}$$

3.3 Upper Bound Group VER

The expression in (3.6) involves two summations to obtain the group VER. To deal with these summations, let $d_{u,min}^2$ denoted as the minimum squared Euclidean distance of the uth group, expressed as (Maza *et al.*, 2020)

$$\begin{aligned} d_{u,min}^2 &= \min_{i,j;\, i \neq j} d_{u,ij}^2 \\ &= \min_{i,j;\, i \neq j} \mathbf{e}_{u,ij}^H \mathbf{B}_u^2 \mathbf{e}_{u,ij}. \end{aligned} \tag{3.7}$$

Therefore, $Q(d_{u,ij}^2)$ can be bounded by $Q(d_{u,min}^2)$, and as a result, we can obtain a closed form for the expression of the group VER in (3.6) as (Maza *et al.*, 2020)

$$PE_u \leq (\mathcal{M}_u - 1)\, Q\left(\sqrt{\frac{d_{u,min}^2}{2}\gamma}\right), \tag{3.8}$$

which is the well-known union-bound performance.

The average PE can be obtained by applying the expected value operation to PE_u, which is a function of a random variable $d_{u,min}^2$. Hence, the distribution of the minimum squared Euclidean distance, $d_{u,min}^2$, is derived in the following section (Maza *et al.*, 2020).

3.4 Distribution of the minimum squared Euclidean distance

We derive the distribution of $d_{u,min}^2$ based on the *multivariate random variable* (refer to Annex I for further details) and *stochastic order* theories. We define the partition and distribution of the

channel and autocorrelation channel matrix. Then, we deduce the distribution of the equivalent squared group whitening matrix and the probability density function of the equivalent minimum squared Euclidean distance.

3.4.1 Channel matrix partition

Let the channel, $\mathbf{H} \in \mathbb{C}^{M\times N}$, and correlation $\mathbf{\Sigma} \in \mathbb{C}^{N\times N}$ matrices, given in (1.9), be partitioned as

$$\mathbf{H} = \begin{pmatrix} \mathbf{H}_u & \mathbf{H}_{\bar{u}} \end{pmatrix} \quad \text{and} \quad \mathbf{\Sigma} = \begin{pmatrix} \mathbf{\Sigma}_u & \mathbf{\Sigma}_{u\bar{u}} \\ \mathbf{\Sigma}_{\bar{u}u} & \mathbf{\Sigma}_{\bar{u}} \end{pmatrix}, \tag{3.9}$$

where $\mathbf{H}_u \in \mathbb{C}^{M\times N_u}$ and $\mathbf{\Sigma}_u \in \mathbb{C}^{N_u\times N_u}$ are the channel and correlation matrices of the uth group, while $\mathbf{H}_{\bar{u}} \in \mathbb{C}^{M\times N_{\bar{u}}}$ and $\mathbf{\Sigma}_{\bar{u}} \in \mathbb{C}^{N_{\bar{u}}\times N_{\bar{u}}}$ are the channel and correlation matrices for the remaining users; $N_{\bar{u}} = N - N_u$. Moreover, $\mathbf{\Sigma}_{u\bar{u}} \in \mathbb{C}^{N_u\times N_{\bar{u}}}$ is the correlation matrix for the UE pertaining to the uth group and the remaining users, and $\mathbf{\Sigma}_{\bar{u}u} = \mathbf{\Sigma}_{u\bar{u}}^H$. Furthermore, when $\mathbf{\Sigma}_{u\bar{u}} = \mathbf{0}$, then $\mathbf{H}_u$ is statistically independent of $\mathbf{H}_{\bar{u}}$, denoted as $\mathbf{H}_u \perp\!\!\!\perp \mathbf{H}_{\bar{u}}$ (Maza *et al.*, 2020).

3.4.2 Autocorrelation channel matrix

Let us consider a channel matrix $\mathbf{H} \in \mathbb{C}^{M\times N}$, with matrix-variate Gaussian distribution denoted as $\mathbf{H} \sim \mathbb{C}\mathcal{N}_{N,M}(\mathbf{0}, \mathbf{I}_M \otimes \mathbf{\Sigma})$, i.e., for distributed antenna layout configuration, with $\mathbf{\Sigma} > 0 \in \mathbb{C}^{N\times N}$. Then, the autocorrelation channel matrix, denoted as $\mathbf{R} = \mathbf{H}^H\mathbf{H} \in \mathbb{C}^{N\times N}$, is a Hermitian positive-definite random matrix, which has a complex central N-dimensional Wishart distribution with M degrees of freedom, and $\mathbf{\Sigma}$ matrix parameters denoted as (Shin & Lee, 2003; Andersen, 2000)

$$\mathbf{R} \sim \mathbb{C}\mathcal{W}_N(M, \mathbf{\Sigma}). \tag{3.10}$$

Then, let $\mathbf{R}$ be partitioned as

$$\mathbf{R} = \begin{pmatrix} \mathbf{R}_u & \mathbf{R}_{u\bar{u}} \\ \mathbf{R}_{\bar{u}u} & \mathbf{R}_{\bar{u}} \end{pmatrix}, \tag{3.11}$$

where $\mathbf{R}_u = \mathbf{H}_u^H \mathbf{H}_u \in \mathbb{C}^{N_u \times N_u}$, $\mathbf{R}_{\bar{u}} = \mathbf{H}_{\bar{u}}^H \mathbf{H}_{\bar{u}} \in \mathbb{C}^{N_{\bar{u}} \times N_{\bar{u}}}$ and $\mathbf{R}_{u\bar{u}} = \mathbf{H}_u^H \mathbf{H}_{\bar{u}} \in \mathbb{C}^{N_u \times N_{\bar{u}}}$; $\mathbf{R}_{\bar{u}u} = \mathbf{R}_{u\bar{u}}^H$. Finally, we notice that $\mathbf{R}_u$ is the squared whitening matrix given in (1.43).

3.4.3 Equivalent squared group whitening matrix

The GD-ML receiver exploits the correlation between UEs in the same group while they are jointly detected. However, it does not consider the correlation between UEs from different groups. Therefore, to obtain a realistic distribution of the minimum squared Euclidean distance, we also need to consider the effect of the correlation among the different groups on the construction on the squared whitening matrix. For this purpose, we should differentiate between the following two cases (Maza *et al.*, 2020):

- *Case 1:* The matrix $\mathbf{R}_u$ is statistically independent of $\mathbf{R}_{\bar{u}}$, denoted as $\mathbf{R}_u \perp\!\!\!\perp \mathbf{R}_{\bar{u}}$ if $\mathbf{\Sigma}_{u\bar{u}} = \mathbf{0}$, which implies $\mathbf{H}_u \perp\!\!\!\perp \mathbf{H}_{\bar{u}}$, as mentioned in subsection 3.4.1 (Andersen, Hojbjerre, Sorensen & Eriksen, 1995; Bilodeau, Brenner & Bilodeau, 1999; Rao, 1965). This implies that the UEs that belong to the uth group are statistically independent of the rest of other UE. In this analysis, we consider a communication system with closely-located and correlated UEs, where the transmit correlation matrix $\mathbf{\Sigma} \neq \mathbf{I}_N$. Then, given the uth group, $\mathbf{\Sigma}_{u\bar{u}} \neq \mathbf{0}$, as a consequence, $\mathbf{R}_u \not\perp\!\!\!\perp \mathbf{R}_{\bar{u}}$. Thus, $\mathbf{R}_u$ does not represent a realistic squared whitening matrix for the proposed system (Maza *et al.*, 2020).
- *Case 2:* To derive a realistic squared whitening matrix, we define the equivalent whitening matrix in the following proposition (Maza *et al.*, 2020):

  ***Proposition* 1.** *Considering the partition of the matrices defined in (3.9) and (3.11), let* $\mathbf{R}_{u_\perp}$ *and* $\mathbf{\Sigma}_{u_\perp}$ *be the equivalent squared whitening and covariance matrices of the uth group respectively, expressed as (Maza* et al.*, 2020)*

$$\mathbf{R}_{u_\perp} = \mathbf{R}_u - \mathbf{R}_{u\bar{u}} \mathbf{R}_{\bar{u}}^{\dagger} \mathbf{R}_{\bar{u}u}, \tag{3.12a}$$

$$\mathbf{\Sigma}_{u_\perp} = \mathbf{\Sigma}_u - \mathbf{\Sigma}_{u\bar{u}} \mathbf{\Sigma}_{\bar{u}}^{\dagger} \mathbf{\Sigma}_{\bar{u}u}. \tag{3.12b}$$

Then, $\mathbf{R}_{u_\perp}$ *has a Wishart distribution denoted by (Maza* et al.*, 2020)*

$$\mathbf{R}_{u_\perp} \sim \mathcal{CW}_{N_u}(L_u, \Sigma_{u_\perp}), \tag{3.13}$$

where $L_u = M - N + N_u$*. Moreover (Maza* et al.*, 2020),*

$$\mathbf{R}_{u_\perp} \perp\!\!\!\perp (\mathbf{R}_{\bar{u}}, \mathbf{R}_{u\bar{u}}), \tag{3.14a}$$

$$\mathbf{\Sigma}_{u_\perp} \perp\!\!\!\perp (\mathbf{\Sigma}_{\bar{u}}, \mathbf{\Sigma}_{u\bar{u}}). \tag{3.14b}$$

Proof. Let $\mathbf{P} = \mathbf{H}_{\bar{u}}(\mathbf{H}_{\bar{u}}^H\mathbf{H}_{\bar{u}})^\dagger\mathbf{H}_{\bar{u}}^H$ and $\mathbf{Q} = \mathbf{I}_M - \mathbf{P}$ be the projection matrices. $\mathbf{PQ} = \mathbf{0}$, $\mathbf{PH}_{\bar{u}} = \mathbf{H}_{\bar{u}}$, and $\mathbf{QH}_{\bar{u}} = \mathbf{0}$. Then, the orthogonal complement to the subspace spanned by the columns of matrix $\mathbf{H}_{\bar{u}}$ (Rao, 1965; Bilodeau *et al.*, 1999; Eaton, 2007; Maza *et al.*, 2020) is expressed as

$$\begin{aligned}\mathbf{H}_u^H\mathbf{Q}\mathbf{H}_u &= \mathbf{H}_u^H(\mathbf{I}_M - \mathbf{P})\mathbf{H}_u \\ &= \mathbf{H}_u^H\mathbf{H}_u - \mathbf{H}_u^H\mathbf{H}_{\bar{u}}(\mathbf{H}_{\bar{u}}^H\mathbf{H}_{\bar{u}})^\dagger\mathbf{H}_{\bar{u}}^H\mathbf{H}_u \\ &= \mathbf{R}_u - \mathbf{R}_{u\bar{u}}\mathbf{R}_{\bar{u}}^\dagger\mathbf{R}_{\bar{u}u},\end{aligned} \tag{3.15}$$

which is the expression given in (3.12a). $\mathbf{R}_{u_\perp}$ is also known as the generalized Schur complement of $\mathbf{R}_{\bar{u}}$ in $\mathbf{R}$. The same criterion is applied to $\mathbf{\Sigma}$ to obtain $\mathbf{\Sigma}_{u_\perp}$ in (3.12b). For $\mathbf{R} \sim \mathbb{C}\mathcal{W}_N(M, \mathbf{\Sigma})$ with $\mathbf{\Sigma} > 0 \in \mathbb{C}^{N\times N}$ and their partitions, given in (3.9) and (3.11), the authors in (Rao, 1965; Bilodeau *et al.*, 1999; Andersen *et al.*, 1995) demonstrated that the Schur complement of $\mathbf{R}_{\bar{u}}$ in $\mathbf{R}$, has a Wishart distribution size N_u, with L_u degrees of freedom and $\mathbf{\Sigma}_{u_\perp}$ matrix parameter denoted as $\mathbf{R}_{u_\perp} \sim \mathbb{C}\mathcal{W}_{N_u}(M - N_{\bar{u}}, \mathbf{\Sigma}_{u_\perp})$. Substituting $M - N_{\bar{u}}$ by $L_u = M - N + N_u$, we obtain (3.13). Besides, $\mathbf{R}_{u_\perp}$ and $(\mathbf{R}_{\bar{u}}, \mathbf{R}_{u\bar{u}})$ are independently distributed (Maza *et al.*, 2020). □

3.4.4 Distribution of the equivalent minimum squared Euclidean distance

Definition 3.1. *Given the equivalent squared whitening matrix* $\mathbf{R}_{u_\perp}$ *in (3.12a), the equivalent squared Euclidean distance can be written as (Maza* et al.*, 2020)*

$$d^2_{u_\perp,ij} = \mathbf{e}^H_{u,ij}\mathbf{R}_{u_\perp}\mathbf{e}_{u,ij}, \tag{3.16}$$

***Proposition* 2.** *The distribution of* $d^2_{u_\perp,ij}$ *defined in (3.16), is said to have a Gamma distribution with* $\alpha = L_u$ *and* $\beta = \frac{1}{2\sigma^2_{u,ij}}$ *shape and rate parameters, respectively, given as (Maza* et al.*, 2020)*

$$d^2_{u_\perp,ij} \sim Gamma\left(L_u, \frac{1}{2\sigma^2_{u,ij}}\right), \tag{3.17}$$

where

$$\sigma^2_{u,ij} = \mathbf{e}^H_{u,ij}\mathbf{\Sigma}_{u_\perp}\mathbf{e}_{u,ij}. \tag{3.18}$$

Proof. Given $\mathbf{R}_{u_\perp} \sim \mathbb{C}\mathcal{W}_{N_u}(L_u, \mathbf{\Sigma}_{u_\perp})$, and let $\mathbf{e}_{u,ij} \in \mathbb{C}^{N_u}$ be any fixed vector. Then, due to the Wishart distribution properties given in Rao (1965) and Izenman (2013), the distribution of (3.16) can be expressed as (Maza *et al.*, 2020)

$$\mathbf{e}^H_{u,ij}\mathbf{R}_{u_\perp}\mathbf{e}_{u,ij} \sim \sigma^2_{u,ij}\chi^2(2L_u) \tag{3.19}$$

for $\mathbf{e}_{u,ij} \neq 0$ and $\mathbf{\Sigma}_{u_\perp} > 0$. Note that the chi-squared is a special case of the Gamma distribution denoted as $\chi^2(2L_u) \sim Gamma(L_u, \frac{1}{2})$, with $\alpha = L_u$ and $\beta = \frac{1}{2}$ parameters. Then (Maza *et al.*, 2020),

$$\sigma^2_{u,ij}\chi^2(2L_u) \sim Gamma(L_u, \frac{1}{2\sigma^2_{u,ij}}) \tag{3.20}$$

□

Definition 3.2 (Integral Stochastic order)**.** *(Tepedelenlioglu, Rajan & Zhang, 2011, Equation (1))*

Let x and y denote random variables with cumulative distribution functions $F_x(\cdot)$ and $F_y(\cdot)$, respectively, and $\mathfrak{G}$ denote a class of real functions $g : \mathbb{R}^+ \to \mathbb{R}$. Let us define the integral stochastic order with respect to $\mathfrak{G}$ as

$$x \leq_{\mathfrak{G}} y \Leftrightarrow \mathbb{E}[g(x)] \leq \mathbb{E}[g(y)], \forall g \in \mathfrak{G}, \tag{3.21}$$

where $\mathfrak{G}$ is a generator of the order $\leq_{\mathfrak{G}}$ (Tepedelenlioglu et al.*, 2011; Maza* et al.*, 2020).*

***Proposition* 3.** *Let $\mathcal{X} = \{x_k\}$, $k = 1, \cdots, E$ be a set of RVs, where $x_k \sim Gamma(L, \frac{1}{2\sigma_k^2})$ has the same distribution as the equivalent Euclidean distance given in (3.17). Let us select $g(x_k) = x_k$ in (3.21), with $\mathbb{E}[g(x_k)] = 2L\sigma_k^2$. Then, we say for a pair-wise of RVs $x_i, x_j \in \mathcal{X}$ for $i \neq j$, the relation holds*

$$x_i \leq_{\mathfrak{G}} x_j \Leftrightarrow \sigma_i^2 \leq \sigma_j^2, \tag{3.22}$$

which implies that the smaller RV is the one that has the smaller σ_k^2 parameter (Maza et al.*, 2020).*

Proof. Let $x_i \sim Gamma(L, \frac{1}{2\sigma_i^2})$ and $x_j \sim Gamma(L, \frac{1}{2\sigma_j^2})$. If $\sigma_i^2 \leq \sigma_j^2$, then

$$\begin{aligned} \mathbb{E}[g(x_i)] &\leq \mathbb{E}[g(x_j)] \\ 2L\sigma_i^2 &\leq 2L\sigma_j^2 \\ \sigma_i^2 &\leq \sigma_j^2, \end{aligned} \tag{3.23}$$

which entails that the function with the smaller RV must have a smaller mean. Substituting (3.23) in (3.21), we can deduce (3.22) (Maza *et al.*, 2020). □

***Proposition* 4.** *The PDF of the minimum squared Euclidean distance with Gamma distribution, denoted as $d_{u,min}^2 \sim Gamma\left(L_u, \frac{1}{2\sigma_{u,min}^2}\right)$, is given by (Maza* et al.*, 2020)*

$$f_x(X) = \frac{1}{\Gamma(L_u)(2\sigma_{u,min}^2)^{L_u}} X^{L_u - 1} e^{-\frac{1}{2\sigma_{u,min}^2} X}, \tag{3.24}$$

where $\Gamma(\cdot)$ *is the Gamma function,* $x = d^2_{u,min}$*, and*

$$\sigma^2_{u,min} = \min_{i,j;\, i \neq j} \mathbf{e}^H_{u,ij} \mathbf{\Sigma}_{u_\perp} \mathbf{e}_{u,ij}. \tag{3.25}$$

Proof. Let $x_{u,k_i} \sim Gamma\left(L_u, \frac{1}{\sigma^2_{u,k_i}}\right)$, $k_i \in \{1, 2, \cdots, E\}$ be a set of RVs. From the results obtained in (3.22), we can sort the set of elements as (Maza *et al.*, 2020)

$$x_{u,k_1} \leq \cdots \leq x_{u,k_E} \Leftrightarrow \sigma^2_{u,k_1} \leq \cdots \leq \sigma^2_{u,k_E}. \tag{3.26}$$

Then, the smallest RV x_{u,k_1} is given by the maximum rate parameter $\frac{1}{2\sigma^2_{u,k_1}}$, and applying the min$(\cdot)$ function to (3.18), we obtain (3.25). Finally, the PDF of the Gamma distribution parameterized by the shape and rate parameters, α and β respectively, is given by (Maza *et al.*, 2020)

$$f_x(X) = \frac{\beta^\alpha}{\Gamma(\alpha)} X^{\alpha-1} e^{-\beta X} \tag{3.27}$$

substituting $\alpha = L_u$ and $\beta = \frac{1}{2\sigma^2_{u,min}}$ yields (3.24). □

3.5 Average Group VER

We derive a closed-form expression for the average PE defined in (3.8). Since the PE_u is a function of an RV $d^2_{u,min}$, the average PE of the uth group is obtained as (Maza *et al.*, 2020)

$$\begin{aligned} \overline{PE}_u &= \mathbb{E}[g(x)] \\ &= \int_0^\infty g(X) f_x(X) dX, \end{aligned} \tag{3.28}$$

where $g(X) = (\mathcal{M}_u - 1)\, Q\left(\sqrt{\frac{X}{2}\gamma}\right)$ and $f_x(X)$ is the PDF of x, given in (3.24), with shape and rate parameters, L_u and $\beta_u = \frac{1}{2\sigma^2_{u,min}}$, respectively. Substituting $g(X)$ and $f_x(X)$ in (3.28), we

obtain (Maza *et al.*, 2020)

$$\overline{PE}_u \leq (\mathcal{M}_u - 1) \int_0^\infty Q\left(\sqrt{\frac{X}{2}\gamma}\right) \frac{\beta_u^{L_u}}{\Gamma(L_u)} X^{L_u-1} e^{-\beta_u X} dX. \tag{3.29}$$

Using the approximation $Q(w) \approx a_1 e^{-b_1 w^2} + a_2 e^{-b_2 w^2}$ for $w > 0$, where $a_1 = 1/12$, $a_2 = 1/4$, $b_1 = 1/2$, and $b_2 = 2/3$ (Chiani, Dardari & Simon, 2003), we get

$$Q\left(\sqrt{\frac{X}{2}\gamma}\right) \approx a_1 e^{-\frac{b_1\gamma}{2}X} + a_2 e^{-\frac{b_2\gamma}{2}X}. \tag{3.30}$$

Consequently, (3.29) can be written as (Maza *et al.*, 2020)

$$\begin{aligned}\overline{PE}_u \lesssim & (\mathcal{M}_u - 1) \int_0^\infty \left(a_1 e^{-\frac{b_1\gamma}{2}X} + a_2 e^{-\frac{b_2\gamma}{2}X}\right) \frac{\beta_u^{L_u}}{\Gamma(L_u)} X^{L_u-1} e^{-\beta_u X} dX \\ = & (\mathcal{M}_u - 1) \left[\int_0^\infty \frac{a_1 \beta_u^{L_u}}{\Gamma(L_u)} X^{L_u-1} e^{-\left(\frac{b_1\gamma}{2}+\beta_u\right)X} dX + \int_0^\infty \frac{a_2 \beta_u^{L_u}}{\Gamma(L_u)} X^{L_u-1} e^{-\left(\frac{b_2\gamma}{2}+\beta_u\right)X} dX\right].\end{aligned} \tag{3.31}$$

Let $\beta_1 = \left(\frac{b_1\gamma}{2} + \beta_u\right)$ and $\beta_2 = \left(\frac{b_2\gamma}{2} + \beta_u\right)$ be the rate parameters of the PDF of the Gamma distribution of two random variables with common shape parameter L_u (Maza *et al.*, 2020). The first and second integrals in (3.31) can be decomposed as

$$\frac{a_1 \beta_u^{L_u}}{\beta_1^{L_u}} \underbrace{\int_0^\infty \frac{\beta_1^{L_u}}{\Gamma(L_u)} X^{L_u-1} e^{-\beta_1 X} dX}_{=1} \tag{3.32a}$$

and

$$\frac{a_2 \beta_u^{L_u}}{\beta_2^{L_u}} \underbrace{\int_0^\infty \frac{\beta_2^{L_u}}{\Gamma(L_u)} X^{L_u-1} e^{-\beta_2 X} dX}_{=1}, \tag{3.32b}$$

respectively. Substituting (3.32a) and (3.32b) into (3.31), we get (Maza *et al.*, 2020)

$$\overline{PE}_u \lesssim (\mathcal{M}_u - 1)\left(\underbrace{\frac{a_1\beta_u^{L_u}}{\beta_1^{L_u}} + \frac{a_2\beta_u^{L_u}}{\beta_2^{L_u}}}_{\eta}\right). \tag{3.33}$$

Replacing β_u, β_1, β_2, γ, and the Q-function approximation coefficients in (3.33), η can be decomposed as (Maza *et al.*, 2020)

$$\begin{aligned}
\eta &= \frac{1}{12\left(2\sigma_{u,min}^2\right)^{L_u}\left(\frac{\frac{1}{2}SNR}{2} + \frac{1}{2\sigma_{u,min}^2}\right)^{L_u}} + \frac{1}{4\left(2\sigma_{u,min}^2\right)^{L_u}\left(\frac{\frac{2}{3}SNR}{2} + \frac{1}{2\sigma_{u,min}^2}\right)^{L_u}} \\
&= \frac{1}{12\left(2\sigma_{u,min}^2\right)^{L_u}\left(\frac{\frac{1}{2}\sigma_{u,min}^2 SRN+1}{2\sigma_{u,min}^2}\right)^{L_u}} + \frac{1}{4\left(2\sigma_{u,min}^2\right)^{L_u}\left(\frac{\frac{2}{3}\sigma_{u,min}^2 SRN+1}{2\sigma_{u,min}^2}\right)^{L_u}} \\
&= \frac{1}{12\left(\frac{\sigma_{u,min}^2}{2}SNR+1\right)^{L_u}} + \frac{1}{4\left(\frac{2\sigma_{u,min}^2}{3}SNR+1\right)^{L_u}}.
\end{aligned} \tag{3.34}$$

Finally, replacing (3.34) in (3.33), the average VER of the uth group can be formulated as (3.35) (Maza *et al.*, 2020).

$$\overline{PE}_u \lesssim (\mathcal{M}_u - 1)\left(\frac{1}{12\left(\frac{\sigma_{u,min}^2}{2}SNR+1\right)^{L_u}} + \frac{1}{4\left(\frac{2\sigma_{u,min}^2}{3}SNR+1\right)^{L_u}}\right). \tag{3.35}$$

From (3.35), it can be deduced that the SNR is scaled by $\sigma_{u,min}^2$, which demonstrates the influence of the correlation of the UE and the independence between the target and remainder groups since $\sigma_{u,min}^2$ depends on $\mathbf{\Sigma}_{u_\perp} \perp\!\!\!\perp (\mathbf{\Sigma}_{\bar{u}}, \mathbf{\Sigma}_{u,\bar{u}})$, which is given in (3.14b). We can also deduce that the average PE exhibits an inverse proportionality with respect to the SNR raised to the power of L_u (Zhu & Murch, 2002), similar to equation (1.3). This result implies that the GD-ML receiver

provides a diversity gain of $M - N + N_u$. Moreover, for $\lambda = 1$, the diversity gain is proportional to the group size, N_u. Furthermore, for $N_u = 1$, the diversity gain of the GD-ML is similar to that of the ZF receiver, namely $M - N + 1$ (Maza *et al.*, 2020).

3.6 Validation of analytical results

We present the simulation results performed in Matlab to validate the derived analytical expression. We assume each UE transmits 4-QAM symbols sequence over the correlated Rayleigh channel with a distributed antenna layout (Maza *et al.*, 2020).

3.6.1 Average Group VER Performance

We consider a massive MU-MIMO system with $\lambda = 1$ to exploit the multiplexing gain given by a large number of antennas, which maximizes the amount of UEs served by the BS using the same frequency-time resources. Figure 3.1 shows the numerical and analytical average group VER performance for an MU-MIMO system with $M = 128$, $N = 128$, $\mathbf{\Sigma}(\rho_t = 0.5)$, and $\mathbf{\Psi} = \mathbf{I}$. We validate the analytical results with the corresponding simulation results for different N_u group sizes. The GD-ML performance is improved when N_u increases. This is because the GD-ML receiver provides a diversity gain of $M - N + N_u$. It is also shown that for small group sizes, the analytical and numerical results remain close (i.e., for $N_u = 1$, the analytical and simulation curves match perfectly, which is equivalent to the ZF receiver). They grow apart as the group size increases, which is a consequence of the upper-bound accuracy limitations. However, the derived average VER expression is useful to evaluate the performance and diversity gain of the GD-ML receivers, which is lacking in the literature (Maza *et al.*, 2020).

3.6.2 Correlation coefficient analysis

In this subsection, we analyze the effect of the correlation between the UEs on the system performance. Figure 3.2 exhibits the performance comparison of the GD-ML receiver for different values of correlation coefficients, with $N_u = 2$, $M = 128$, and $N = 128$. It is observed

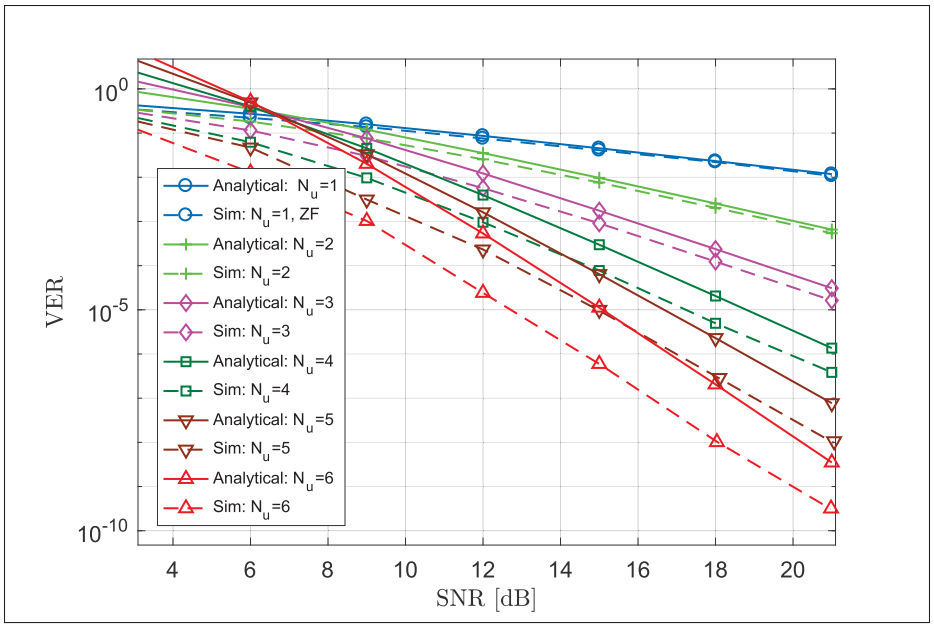

Figure 3.1 Analytical average group VER and simulation results of the GD-ML receivers with group sizes $N_u = \{1, 2, 3, 4, 5, 6\}$, for full load massive MIMO with $M = 128$ and $N = 128$, and $\mathbf{\Sigma}(\rho_t = 0.5)$
Taken from Maza et al. (2020, p.45660)

that the average VER given in (3.35) is degraded when ρ_t increases. We can also observe that for a moderate SNR, the derived expression closely matches the numerical results, especially for high values of ρ_t. To analyze these results, we start from the transmit covariance matrix given in (1.12), which depends on ρ_t, then (3.12b) is also a function of ρ_t. As a result, (3.25) can be written as (Maza *et al.*, 2020)

$$\sigma^2_{u,min}(\rho_t) = \min_{i,j;\, i \neq j} \mathbf{e}^H_{u,ij} \mathbf{\Sigma}_{u_\perp}(\rho_t) \mathbf{e}_{u,ij}. \tag{3.36}$$

Figure 3.3 shows the result of (3.36), where we observe that $\sigma^2_{u,min}(\rho_t)$ is inversely proportional to ρ_t. Thus, in (3.35), $\sigma^2_{u,min}(\rho_t)$ scales the SNR, which implies that the performance is improved

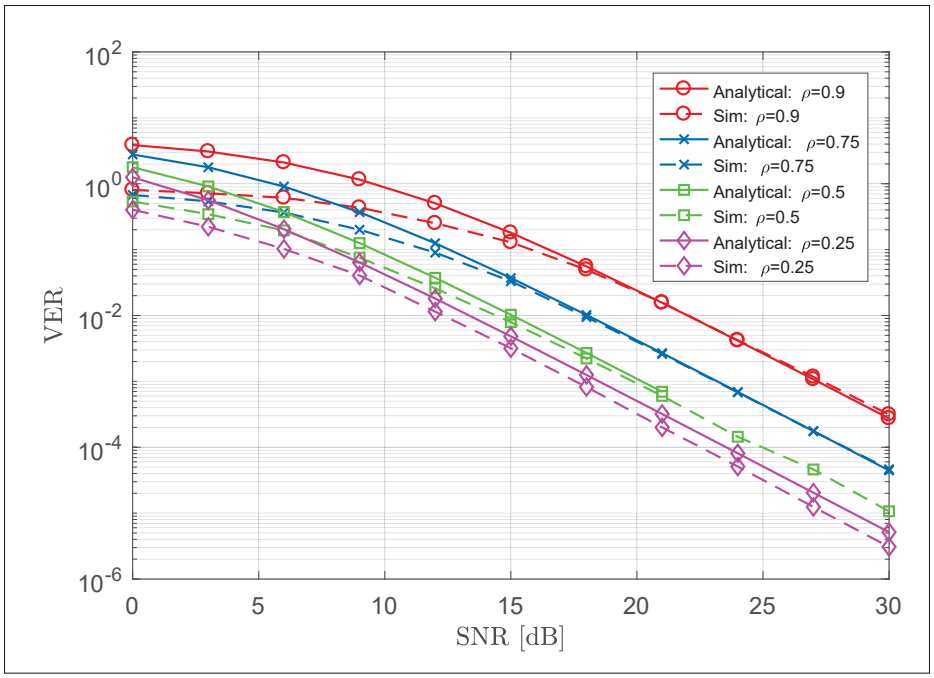

Figure 3.2 Performance comparison for different correlation coefficients ρ_t, for $M = 128$, $N = 128$, and GD-ML with group size $N_u = 2$
Taken from Maza et al. (2020, p.45661)

when ρ_t is decreased. Additionally, if $\rho_t \to 0$, then $\mathbf{\Sigma}_{u\bar{u}}(\rho_t) = \mathbf{\Sigma}_{\bar{u}u}(\rho_t) \approx \mathbf{0}$ in (3.12b), which corresponds to a negligible inter-group interference (Maza *et al.*, 2020).

3.6.3 Diversity gain and complexity analysis

We consider an $M = 128$ and $N = 128$ MU-MIMO system with distributed antenna layout configuration. Then, the ZF and MMSE receivers provide a unitary diversity gain with a complexity of 8.41×10^6 and 8.42×10^6 FLOPs, respectively. In contrast, the GD-ML receiver with $N_u = 5$ provides a diversity gain of 5 at the cost of 8.47×10^6 FLOPs (meeting the complexity criterion given in Chapter 1).

If we want the ZF and MMSE receivers to archive a diversity order of 5, it is necessary to add 4 additional antennas, i.e., $M = 132$ antennas at the BS. This addition involves an extra hardware

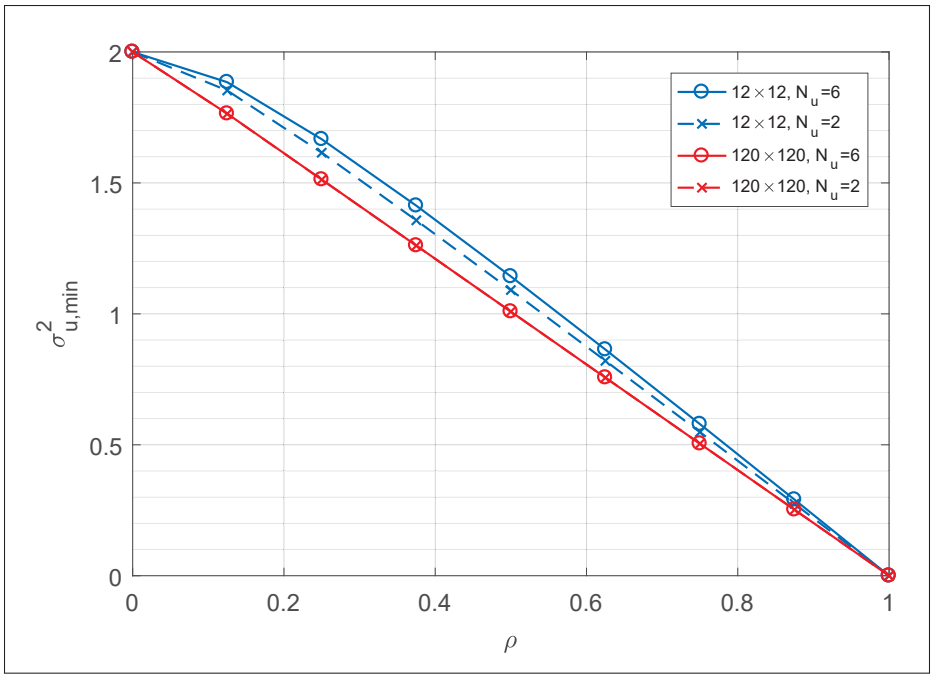

Figure 3.3 $\sigma^2_{u,min}$ vs. ρ comparison, for 12×12, 128×128 MU-MIMO systems, and GD-ML with $N_u = \{2, 6\}$
Taken from Maza et al. (2020, p.45661)

implementation and a complexity of 8.61×10^6 and 8.62×10^6 FLOPs for ZF and MMSE, respectively, which result in a higher complexity compered to the GD-ML.

CONCLUSION AND RECOMMENDATIONS

Large MU-MIMO systems provide enormous multiplexing gains with a full load factor, making them a desirable solution to meet the high connection needs of the 5G and B5G networks. However, under the full-load factor, the performance of linear receivers is severely degraded due to unfavorable propagation conditions, highlighting the need for exploring more efficient solutions.

The GD-ML technique enhances the performance of linear receivers without adding excessive complexity. The literature review revealed that this technique has been widely studied for conventional MIMO systems with ideal channels; however, its potential for large MU-MIMO systems with realistic channels remains unexplored. With this motivation, in this thesis, we explored the efficiency of the GD-ML receiver in large MU-MIMO systems. We derived the performance and complexity analysis assuming full-load factors and correlated channels. In the following, we summarize the main contribution of this thesis.

We first discussed the background of wireless communication systems, emphasizing on fading and diversity. We studied MIMO techniques, focusing on diversity and spatial multiplexing and their benefits in terms of array, diversity, and multiplexing gains. We also discussed uplink and downlink MU-MIMO systems and their advantages over conventional MIMO systems. We provided an overview of correlated MU-MIMO channel models. We also presented and compared linear and non-linear MU-MIMO receivers in complexity and performance. Finally, we examined the main concepts and challenges behind large MU-MIMO systems.

We examined the GD-ML receiver's structure, which includes linear projection, grouping, and ML detection for each group. We also provided numerical results for the GD-ML BER performance with various group sizes. The results demonstrated that GD-ML outperforms ZF and MMSE receivers, even with small group sizes.

We formulated an equation for the hardware complexity of the GD-ML receiver in terms of FLOPs. We presented a complexity criterion for assessing the balance between complexity and performance. Our findings indicate that the grouping and ML detection stages' complexity is negligible compared to the linear transformation stage, which involves channel matrix inversion. We show that for large MU-MIMO systems, the complexity of the GD-ML receivers with small groups size is almost the same as that of the ZF and MMSE. Furthermore, our research demonstrates that for large MU-MIMO systems, the complexity of GD-ML receivers with small group sizes is comparable to that of ZF and MMSE.

We derived a closed-form expression for the average group VER of the GD-ML receiver, with group sizeN_u, for a scenario with N closely-located and correlated UEs at the transmitter side and M uncorrelated distributed antennas at the BS. Our research showed that the GD-ML receiver provides greater diversity gains than linear receivers, where the gain is proportional to $M-N+N_u$. We also found that the GD-ML's performance deteriorates when correlation between the UEs' channels increases. The simulation results validated the derived analytical expression and exhibited that, for small group sizes, the closed-from expression and the numerical outcomes are quite close. Furthermore, we observed that the analytical expression closely matches the numerical results for moderate SNRs values and becomes perfect as the UEs' channel correlation increases.

Future work

In this research, we considered the group VER performance metric for uncoded, distributed large MU-MIMO systems with correlation only at the transmitter side and a fixed grouping strategy. However, the performance expression presented can be further explored to create a more generalized metric that includes a fully correlated channel and different grouping methods.

The GD-ML performance metric considered in this research work is the group VER for uncoded, distributed large MU-MIMO systems with correlation only at the transmitter side and fixed

groping strategy. However, the presented performance expression may be extended to a more generalized metric with fully correlated channels and considering different the grouping methods.

Nonetheless, we have identified several potential areas for future research based on this thesis, including:

- Exploring the correlation on both transmitter and receiver sides.
- Developing an analytical expression for the BER or SER performance metrics.
- Examining scenarios involving coding systems.
- Developing a novel grouping strategy utilizing artificial intelligence.
- Exploring hardware implementation of the GD-ML receiver.

ANNEX I

MULTIVARIATE DISTRIBUTION

We provide a detailed review of multivariate complex random variables, including the distribution of complex random vectors and matrices and essential properties needed to develop the MIMO systems model and derive receiver performance. This annex presents notation used, the complex multivariate Gaussian distribution, and the Wishart distribution.

1. Notation and operations

Let $\mathbf{X} \in \mathbb{C}^{M\times N}$ be a complex random matrix denoted by

$$\mathbf{X} = \begin{array}{c} \begin{matrix} \mathbf{x}_1 & \cdots & \mathbf{x}_N \end{matrix} \\ \begin{pmatrix} X_{11} & \cdots & X_{1N} \\ \vdots & \cdots & \vdots \\ X_{M1} & \cdots & X_{MN} \end{pmatrix} \end{array} \begin{matrix} \mathbf{y}_1^T \\ \vdots \\ \mathbf{y}_M^T, \end{matrix} \tag{A I-1}$$

where $\mathbf{x}_i = [X_{1i}, \cdots, X_{Mi}]^T$ and $\mathbf{y} = \left[X_{j1}, \cdots, X_{jN}\right]^T$ are the ith column and jth row vectors of $\mathbf{X}$ matrix, respectively.

Let $\mathbb{E}[\cdot]$ and $\mathbb{V}[\cdot]$ denote as expectation and variance operators, respectively. Thus, the mean and covariance matrices of $\mathbf{x}$, $\mathbf{y}$, and $\mathbf{X}$ are given by

$$\mathbf{m} = \mathbb{E}[\mathbf{x}], \qquad \mathbf{\Sigma} = \mathbb{V}[\mathbf{x}] \tag{A I-2}$$

$$\mathbf{p} = \mathbb{E}[\mathbf{y}], \qquad \mathbf{\Psi} = \mathbb{V}[\mathbf{y}] \tag{A I-3}$$

$$\mathbf{M} = \mathbb{E}[\mathbf{X}], \qquad \mathbf{\Psi} \otimes \mathbf{\Sigma} = \mathbb{V}[\mathbf{X}], \tag{A I-4}$$

where $\mathbf{\Sigma} \in \mathbb{C}^{N\times N} > 0$, $\mathbf{\Psi} \in \mathbb{C}^{M\times M} > 0$, and $\mathbf{\Psi} \otimes \mathbf{\Sigma} \in \mathbb{C}^{NM\times NM} > 0$ are Hermitian matrices. $\mathbf{m} \in \mathbb{C}^N$, $\mathbf{p} \in \mathbb{C}^M$, and $\mathbf{M} \in \mathbb{C}^{M\times N}$.

2. Complex multivariate Gaussian distribution

A random vector $\mathbf{x} \in \mathbb{C}^N$ is defined as the complex N-variate Gaussian distribution with mean vector $\mathbf{m} \in \mathbb{C}^N$ and covariance matrix $\mathbf{\Sigma} \in \mathbb{C}^{N\times N} > 0$, denoted by

$$\mathbf{x} \sim \mathbb{C}\mathcal{N}_N(\mathbf{m}, \mathbf{\Sigma}), \tag{A I-5}$$

A random matrix $\mathbf{X} \in \mathbb{C}^{M\times N}$ is said to have a matrix-variate Gaussian distribution with mean $\mathbf{M} \in \mathbb{C}^{M\times N}$ and covariance $\mathbf{\Psi} \otimes \mathbf{\Sigma} \in \mathbb{C}^{NM\times NM} > 0$ denoted by

$$\mathbf{X} \sim C\mathcal{N}_{N,M}(\mathbf{M}, \mathbf{\Psi} \otimes \mathbf{\Sigma}), \tag{A I-6}$$

Let $\mathbf{X} \in \mathbb{C}^{M\times N} \sim C\mathcal{N}_{N,M}(\mathbf{0}, \mathbf{I}_M \otimes \mathbf{\Sigma})$, where $\mathbf{I}_M$ is the identity matrix. Then, $\mathbf{X}$ and $\mathbf{\Sigma}$ can be partitioned as

$$\mathbf{X} = \begin{pmatrix} \mathbf{X}_1 & \mathbf{X}_2 \end{pmatrix} \quad , \quad \mathbf{\Sigma} = \begin{pmatrix} \mathbf{\Sigma}_{11} & \mathbf{\Sigma}_{12} \\ \mathbf{\Sigma}_{21} & \mathbf{\Sigma}_{22} \end{pmatrix}, \tag{A I-7}$$

where $\mathbf{X}_j$ is $(M \times r_j)$, and $\mathbf{\Sigma}_{jk}$, size $(r_j \times r_k)$, for $j, k = 1, 2$ and $r = r_1 + r_2$; $\mathbf{\Sigma}_{12}^H = \mathbf{\Sigma}_{21}$. It holds that:

i. $\mathbf{X}_j \sim \mathbb{C}\mathcal{N}_{M\times r_j}(\mathbf{0}_j, \mathbf{I}_M \otimes \mathbf{\Sigma}_{jj})$,

ii. $\mathbf{X}_1$ and $\mathbf{X}_2$ are independent if $\mathbf{\Sigma}_{12} = \mathbf{0}$,

iii. $\mathbf{X}_1 - \mathbf{X}_2\mathbf{\Sigma}_{22}^{\dagger}\mathbf{\Sigma}_{21} \sim \mathbb{C}\mathcal{N}_{M\times r_1}(\mathbf{0}_1, \mathbf{I} \otimes (\mathbf{\Sigma}_{11} - \mathbf{\Sigma}_{12}\mathbf{\Sigma}_{22}^{\dagger}\mathbf{\Sigma}_{21}))$, and $(\mathbf{X}_1 - \mathbf{X}_2\mathbf{\Sigma}_{22}^{\dagger}\mathbf{\Sigma}_{21}) \perp\!\!\!\perp \mathbf{X}_2$.

3. Complex Wishart distribution

Let us consider a random matrix $\mathbf{X} \in \mathbb{C}^{M\times N}$, with matrix-variate Gaussian distribution $\mathbf{X} \sim \mathcal{CN}_{N,M}(\mathbf{0}, \mathbf{I}_M \otimes \mathbf{\Sigma})$. Then, $\mathbf{Z} = \mathbf{X}^H\mathbf{X} \in \mathbb{C}^{N\times N}$ is a Hermitian positive-definite random matrix which have a complex central Wishart distribution with M degrees of freedom, and $\mathbf{\Sigma}$ matrix parameters denoted as (Shin & Lee, 2003; Andersen, 2000)

$$\mathbf{Z} \sim \mathbb{C}\mathcal{W}_N(M, \mathbf{\Sigma}) \tag{A I-8}$$

We present some useful results about Wishart matrices:

i. For $N = 1$ and $\mathbf{\Sigma} = \sigma^2$, the distribution of a complex Wishart matrix yields to $\mathbf{Z} \sim \mathbb{C}\mathcal{W}_1(M, \sigma^2)$, which is also a chi-square distribution with $2M$ degrees of freedom given as

$$\mathbf{Y} \sim \frac{\sigma^2}{2}\chi^2(2M). \tag{A I-9}$$

ii. Let $\mathbf{Z} \sim \mathbb{C}\mathcal{W}_N(M, \mathbf{\Sigma})$ with $\mathbf{\Sigma} > \mathbf{0}$ and $\mathbf{b} \neq \mathbf{0} \in \mathbb{C}^N$ be a deterministic vector. Then, $\mathbf{b}^H\mathbf{Z}\mathbf{b}$ is a chi-square distribution expressed as $\mathbf{b}^H\mathbf{Z}\mathbf{b} \sim \sigma_b^2\chi^2(2M)$ (Pavur, 1980), where $\sigma_b^2 = \mathbf{b}^H\mathbf{\Sigma}\mathbf{b}$. Applying the scaling property of gamma and chi-square distributions, $\mathbf{b}^H\mathbf{Y}\mathbf{b}$ is said to have a gamma distribution with $\alpha = M$ shape and $\beta = \frac{1}{2\sigma_b^2}$ rate parameters denoted as

$$\mathbf{b}^H\mathbf{Y}\mathbf{b} \sim Gamma\,(\alpha, \beta) \tag{A I-10}$$

iii. Let consider the partition of $\mathbf{X}$, $\mathbf{Y}$ and $\mathbf{\Sigma}$, then

$$\mathbf{X} = \begin{pmatrix} \mathbf{X}_1 & \mathbf{X}_2 \end{pmatrix}, \quad \mathbf{Y} = \begin{pmatrix} \mathbf{Y}_{11} & \mathbf{Y}_{12} \\ \mathbf{Y}_{21} & \mathbf{Y}_{22} \end{pmatrix} \text{ and } \mathbf{\Sigma} = \begin{pmatrix} \mathbf{\Sigma}_{11} & \mathbf{\Sigma}_{12} \\ \mathbf{\Sigma}_{21} & \mathbf{\Sigma}_{22} \end{pmatrix}, \tag{A I-11}$$

where $\mathbf{X}_j$ and $\mathbf{X}_k$ are the $(M \times N_j)$ and $(M \times N_k)$ matrices respectively, $\mathbf{Y}_{jk}$ and $\mathbf{\Sigma}_{jk}$, size $(N_j \times N_k)$ for $j, k = 1, 2$; $N = N_j + N_k$,. Then, $\mathbf{Y}_{jk} = \mathbf{Y}_{kj}^H$ and $\mathbf{\Sigma}_{jk} = \mathbf{\Sigma}_{kj}^H$. Moreover, $\mathbf{Y}_{jj} = \mathbf{X}_j\mathbf{X}_j^H$, and $\mathbf{Y}_{kk} = \mathbf{X}_k\mathbf{X}_k^H$ (Bilodeau *et al.*, 1999). Then, the distribution of

$\mathbf{Y}_{11.2} = \mathbf{Y}_{11} - \mathbf{Y}_{12}\mathbf{Y}_{22}^{\dagger}\mathbf{Y}_{21}$ called the generalized Schuar complement of $\mathbf{Y}_{22}$ in $\mathbf{Y}$ is given by

$$\mathbf{Y}_{11.2} \sim \mathbb{C}\mathcal{W}_{N_1}(M - N_2, \mathbf{\Sigma}_{11.2}) \tag{A I-12}$$

where $\mathbf{\Sigma}_{11.2} = \mathbf{\Sigma}_{11} - \mathbf{\Sigma}_{12}\mathbf{\Sigma}_{22}^{\dagger}\mathbf{\Sigma}_{21}$, and

$$\mathbf{Y}_{22} \sim \mathbb{C}\mathcal{W}_{N_1}(M, \mathbf{\Sigma}_{22}) \tag{A I-13}$$

$$\mathbf{Y}_{11.2} \perp\!\!\!\perp (\mathbf{Y}_{21}, \mathbf{Y}_{22}) \tag{A I-14}$$

where $a \perp\!\!\!\perp b$ denotes the statistical independence between a and b.

BIBLIOGRAPHY

Almers, P., Bonek, E., Burr, A., Czink, N., Debbah, M., Degli-Esposti, V., Hofstetter, H., Kyösti, P., Laurenson, D., Matz, G., Molisch, A. F., Oestges, C. & Özcelik, H. (2007). Survey of Channel and Radio Propagation Models for Wireless MIMO Systems. *EURASIP Journal on Wireless Communications and Networking*, 2007(1), 019070. doi: 10.1155/2007/19070.

Andersen, H. H., Hojbjerre, M., Sorensen, D. & Eriksen, P. S. (1995). The Complex Wishart Distribution and the Complex U-distribution. In *Linear and Graphical Models: for the Multivariate Complex Normal Distribution* (pp. 39–66). New York, NY: Springer New York. doi: 10.1007/978-1-4612-4240-6_3.

Andersen, J. B. (2000). Array gain and capacity for known random channels with multiple element arrays at both ends. *IEEE Journal on Selected Areas in Communications*, 18(11), 2172–2178. doi: 10.1109/49.895022.

Banafaa, M., Shayea, I., Din, J., Hadri Azmi, M., Alashbi, A., Ibrahim Daradkeh, Y. & Alhammadi, A. (2023). 6G Mobile Communication Technology: Requirements, Targets, Applications, Challenges, Advantages, and Opportunities. *Alexandria Engineering Journal*, 64, 245–274. doi: 10.1016/j.aej.2022.08.017.

Barry, J., Lee, E. & Messerschmitt, D. (2004). *Digital Communication* (ed. illustrated). Springer Science & Business Media.

Bayramoglu, M. F., Karjalainen, M. & Juntti, M. (2013). Mitigation of inter-symbol interference in single-carrier FDMA via group detection. *2013 IEEE Global Conference on Signal and Information Processing*, pp. 1218–1221. doi: 10.1109/GlobalSIP.2013.6737127.

Bilodeau, M., Brenner, D. & Bilodeau, M. (1999). *Theory of multivariate statistics*.

Björnson, E., Hoydis, J., Kountouris, M. & Debbah, M. (2014). Massive MIMO Systems With Non-Ideal Hardware: Energy Efficiency, Estimation, and Capacity Limits. *IEEE Transactions on Information Theory*, 60(11), 7112–7139. doi: 10.1109/TIT.2014.2354403.

Björnson, E., Hoydis, J. & Sanguinetti, L. (2017). Massive MIMO Networks: Spectral, Energy, and Hardware Efficiency. *Foundations and Trends® in Signal Processing*, 11(3-4), 154–655. doi: 10.1561/2000000093.

Bottomley, G. E. & Wang, Y.-E. (2010). A Novel Multistage Group Detection Technique and Applications. *IEEE Transactions on Wireless Communications*, 9(8), 2438–2443. doi: 10.1109/TWC.2010.061710.091460.

Cal-Braz, J. & Sampaio-Neto, R. (2014). Nested Maximum Likelihood Group Detection in Generalized Spatial Modulation MIMO Systems. *IEEE Communications Letters*, 18(6), 953–956. doi: 10.1109/LCOMM.2014.2323252.

Chaudhari, Q. (2021). *5G Physical Layer*. Melbourne, Australia.

Chiani, M., Dardari, D. & Simon, M. (2003). New exponential bounds and approximations for the computation of error probability in fading channels. *IEEE Transactions on Wireless Communications*, 24(5), 840–845. doi: 10.1109/TWC.2003.814350.

Cho, Y., Kim, J., Yang, W. & Kang, C. (2010). *MIMO-OFDM Wireless Communications with MATLAB*. John Wiley and Sons. doi: 10.1002/9780470825631.

Chockalingam, A. & Rajan, B. S. (2013). *Large MIMO Systems*. Cambridge: Cambridge University Press. doi: 10.1017/CBO9781139208437.

Choi, J. W., Shim, B., Singer, A. C. & Cho, N. I. (2010). Low-Complexity Decoding via Reduced Dimension Maximum-Likelihood Search. *IEEE Transactions on Signal Processing*, 58(3), 1780–1793. doi: 10.1109/TSP.2009.2036482.

Choi, J. W., Lee, B., Shim, B. & Kang, I. (2013). Low complexity soft-input soft-output group detection for massive MIMO systems. *2013 IEEE International Conference on Communications (ICC)*, pp. 4792–4796. doi: 10.1109/ICC.2013.6655332.

Choi, W.-J., Negi, R. & Cioffi, J. (2000). Combined ML and DFE decoding for the V-BLAST system. *2000 IEEE International Conference on Communications. ICC 2000. Global Convergence Through Communications. Conference Record*, 3, 1243–1248 vol.3. doi: 10.1109/ICC.2000.853698.

Dalal, U. (2021). *Wireless Communication and Networks* [Version Knovel]. Oxford University Press. Retrieved from: https://app.knovel.com/hotlink/toc/id:kpWCN00011/wireless-communication/wireless-communication.

Darbari, F., Stewart, R. W. & Glover, I. A. (2010). MIMO Channel Modelling. In *Signal Processing*.

Eaton, M. L. (2007). Chapter 8: The Wishart Distribution. In *Multivariate Statistics: A Vector Space Approach.* (pp. 302–333). Beachwood, Ohio, USA: Institute of Mathematical Statistics.

Elijah, O., Abdul Rahim, S. K., New, W. K., Leow, C. Y., Cumanan, K. & Kim Geok, T. (2022). Intelligent Massive MIMO Systems for Beyond 5G Networks: An Overview and Future Trends. *IEEE Access*, 10, 102532–102563. doi: 10.1109/ACCESS.2022.3208284.

Elkhazin, A., Plataniotis, K. & Pasupathy, S. (2006). Reduced-dimension MAP turbo-BLAST detection. *IEEE Transactions on Communications*, 54(1), 108–118. doi: 10.1109/TCOMM.2005.861658. Conference Name: IEEE Transactions on Communications.

Flordelis, J., Rusek, F., Gao, X., Dahman, G., Edfors, O. & Tufvesson, F. (2018). Spatial Separation of Closely-Located Users in Measured Massive MIMO Channels. *IEEE Access*, 6, 40253–40266. doi: 10.1109/ACCESS.2018.2854307.

Foschini, G. J. (1996). Layered space-time architecture for wireless communication in a fading environment when using multi-element antennas. *Bell Labs Technical Journal*, 1(2), 41–59. doi: 10.1002/bltj.2015.

Gao, X., Jiang, B., Li, X., Gershman, A. B. & McKay, M. R. (2009). Statistical Eigenmode Transmission Over Jointly Correlated MIMO Channels. *IEEE Transactions on Information Theory*, 55(8), 3735–3750. doi: 10.1109/TIT.2009.2023737.

Goldsmith, A. (2005). *Wireless Communications*. Cambridge: Cambridge University Press. doi: 10.1017/CBO9780511841224.

Grant, S. J. & Cavers, J. K. (2000). Further analytical results on the joint detection of cochannel signals using diversity arrays. *IEEE Transactions on Communications*, 48(11), 1788–1792. doi: 10.1109/26.886468.

Hunger, R. (2007). *Floating Point Operations in Matrix-Vector Calculus*.

Izenman, A. J. (2013). *Modern multivariate statistical techniques: regression, classification, and manifold learning* (ed. Corrected at 2. printing). New York: Springer.

Jald en, J. (2004). Maximum Likelihood Detection for the Linear MIMO Channel.pdf [Licentiate Thesis]. Stockholm, Sweden. Retrieved on 2017-11-02 from: https://www.diva-portal.org/smash/get/diva2:14228/FULLTEXT01.pdf.

Jeon, Y.-S., Hong, S.-N. & Lee, N. (2017). Blind detection for MIMO systems with low-resolution ADCs using supervised learning. *2017 IEEE International Conference on Communications (ICC)*, pp. 1–6. doi: 10.1109/ICC.2017.7997434.

Jiang, R. & Liu, Y.-F. (2021). Antenna Efficiency in Massive MIMO Detection. *2021 IEEE 22nd International Workshop on Signal Processing Advances in Wireless Communications (SPAWC)*, pp. 51–55. doi: 10.1109/SPAWC51858.2021.9593196.

Kamga, G. N., Xia, M. & Aïssa, S. (2016). Spectral-Efficiency Analysis of Massive MIMO Systems in Centralized and Distributed Schemes. *IEEE Transactions on Communications*, 64(5), 1930–1941. doi: 10.1109/TCOMM.2016.2519513.

Karipidis, E. (2015). *D1.1 System scenarios and requirements specifications* (Report n°ICT-619086-D1.1 MAMMOET). Retrieved on 2019-11-30 from: https://mammoet-project.eu/downloads/publications/deliverables/MAMMOET-D1.1-Scenarios-Requirements-PU-M12.pdf.

Krause, M., Taylor, D. P. & Martin, P. A. (2011). List-Based Group-Wise Symbol Detection for Multiple Signal Communications. *IEEE Transactions on Wireless Communications*, 10(5), 1636–1644. doi: 10.1109/TWC.2011.041211.101164.

Kumar, S. (2022). 6G Mobile Communication Networks: Key Services and Enabling Technologies. *JICTS*. doi: 10.13052/jicts2245-800X.1011.

Li, X., Huang, H. C., Lozano, A. & Foschini, G. J. (2000). Reduced-complexity detection algorithms for systems using multi-element arrays. *Globecom '00 - IEEE. Global Telecommunications Conference. Conference Record (Cat. No.00CH37137)*, 2, 1072–1076 vol.2. doi: 10.1109/GLOCOM.2000.891302.

Liu, J., Yang, X., Sun, Q., Zhang, R. & Qian, Y. (2022). Hybrid Beamforming Grouping Sum-Rate Maximization Algorithm for Multiuser mmWave Massive MIMO Systems. *International Journal of Digital Multimedia Broadcasting*, 2022, 1–12. doi: 10.1155/2022/2865659.

Loyka, S. & Gagnon, F. (2004). Performance analysis of the V-BLAST algorithm: an analytical approach. *IEEE Transactions on Wireless Communications*, 3(4), 1326–1337. doi: 10.1109/TWC.2004.830853.

Loyka, S. L. (2001). Channel capacity of MIMO architecture using the exponential correlation matrix. *IEEE Communications Letters*, 5(9), 369–371. doi: 10.1109/4234.951380.

Mandloi, M., Gurjar, D., Pattanayak, P. & Nguyen, H. (Eds.). (2021). *5G and Beyond Wireless Systems: PHY Layer Perspective*. Singapore: Springer Singapore. doi: 10.1007/978-981-15-6390-4.

Marzetta, T. L. (2010). Noncooperative Cellular Wireless with Unlimited Numbers of Base Station Antennas. *IEEE Transactions on Wireless Communications*, 9(11), 3590–3600. doi: 10.1109/TWC.2010.092810.091092.

Maza, B. P., Dahman, G., Kaddoum, G. & Gagnon, F. (2020). Average Vector-Symbol Error Rate Closed-Form Expression for ML Group Detection Receivers in Large MU-MIMO Channels With Transmit Correlation. *IEEE Access*, 8, 45653–45663. doi: 10.1109/ACCESS.2020.2977840.

Maza, B., Sampaio-Neto, R. & Medina, C. (2012). Detecção Ótima por Grupos em Sistemas com Transmissão em Blocos. *Anais do XXX SBrT'12*, pp. 98811.

Mehana, A. H. & Nosratinia, A. (2010). Diversity of MMSE MIMO receivers. *2010 IEEE International Symposium on Information Theory*, pp. 2163–2167. doi: 10.1109/ISIT.2010.5513458.

Moon, S., Jeong, J., Lee, H. & Lee, I. (2010). Enhanced Groupwise Detection with a New Receive Combiner for Spatial Multiplexing MIMO Systems. *IEEE Transactions on Communications*, 58(9), 2511–2515. doi: 10.1109/TCOMM.2010.09.090135.

Naeem, F., Ali, M., Kaddoum, G., Huang, C. & Yuen, C. (2023). Security and Privacy for Reconfigurable Intelligent Surface in 6G: A Review of Prospective Applications and Challenges. *IEEE Open Journal of the Communications Society*, 4, 1196–1217. doi: 10.1109/OJCOMS.2023.3273507. Conference Name: IEEE Open Journal of the Communications Society.

Nee, R. v., Zelst, A. v. & Awater, G. (2000). Maximum likelihood decoding in a space division multiplexing system. *VTC2000-Spring. 2000 IEEE 51st Vehicular Technology Conference Proceedings (Cat. No.00CH37026)*, 1, 6–10 vol.1. doi: 10.1109/VETECS.2000.851407.

Ngo, H. Q., Larsson, E. G. & Marzetta, T. L. (2014). Aspects of favorable propagation in Massive MIMO. *2014 22nd European Signal Processing Conference (EUSIPCO)*, pp. 76–80.

Nguyen, T.-B., Le, M.-T., Ngo, V.-D., Nguyen, T.-D. & Han, H.-D. (2018a). Efficient Detectors based on Group Detection for Massive MIMO systems. *REV Journal on Electronics and Communications*. doi: 10.21553/rev-jec.167.

Nguyen, T.-B., Le, M.-T., Ngo, V.-D. & Nguyen, V.-G. (2018b). Parallel Group Detection Approach for Massive MIMO systems. *2018 International Conference on Advanced Technologies for Communications (ATC)*, pp. 94–99. doi: 10.1109/ATC.2018.8587606.

Osseiran, A., Boccardi, F., Braun, V., Kusume, K., Marsch, P., Maternia, M., Queseth, O., Schellmann, M., Schotten, H., Taoka, H., Tullberg, H., Uusitalo, M. A., Timus, B. & Fallgren, M. (2014). Scenarios for 5G mobile and wireless communications: the vision of the METIS project. *IEEE Communications Magazine*, 52(5), 26–35. doi: 10.1109/MCOM.2014.6815890.

Panno, D. & Riolo, S. (2019). A New Centralized Access Control Scheme for D2D-Enabled mmWave Networks. *IEEE Access*, 7, 80697–80716. doi: 10.1109/ACCESS.2019.2923599.

Pavan, G., Reddy, V. K. R. N., Prasad, A. R., Chintala, R. R. & Sai, N. R. (2023). A Comprehensive Survey on Recent Advances in 5G Networks and Mobile Systems. *2023 7th International Conference on Computing Methodologies and Communication (ICCMC)*, pp. 949-953. doi: 10.1109/ICCMC56507.2023.10083901.

Pavur, R. (1980). Quadratic forms involving the complex Gaussian. Montreal.

Proakis, J. & Salehi, M. (2008). *Digital Communications* (ed. 5). McGrow-Hill.

Rao, C. R. (1965). *Linear Statistical Inference and its Applications* (ed. Second). USA: John Wiley & Sons.

Rappaport, T. S. (2002). *Wireless Communications: Principles and Practice* (ed. Second). Upper Saddle River, N.J.: Pearson.

Razi, A., Ryan, D. J., Yuan, J. & Collings, I. B. (2010). Performance of Vector Perturbation Multiuser MIMO Systems over Correlated Channels. *2010 IEEE Wireless Communication and Networking Conference*, pp. 1–5. doi: 10.1109/WCNC.2010.5506749.

Sfar, S. & Letaief, K. B. (2003). Group ordered successive interference cancellation for multiuser detection in MIMO CDMA systems. *2003 IEEE Wireless Communications and Networking, 2003. WCNC 2003.*, 2, 888–893 vol.2. doi: 10.1109/WCNC.2003.1200489.

Sfar, S., Dai, L. & Letaief, K. (2005). Optimal Diversity-Multiplexing Tradeoff With Group Detection for MIMO Systems. *IEEE Transactions on Communications*, 53(7), 1178–1190. doi: 10.1109/TCOMM.2005.851596.

Shin, H. & Lee, J. H. (2003). Capacity of multiple-antenna fading channels: spatial fading correlation, double scattering, and keyhole. *IEEE Transactions on Information Theory*, 49(10), 2636–2647. doi: 10.1109/TIT.2003.817439.

Shiu, D.-S., Foschini, G. J., Gans, M. J. & Kahn, J. M. (2000). Fading correlation and its effect on the capacity of multielement antenna systems. *IEEE Transactions on Communications*, 48(3), 502–513. doi: 10.1109/26.837052.

Simon, M. K. & Alouini, M.-S. (2000). *Digital communication over fading channels: a unified approach to performance analysis*. New York: John Wiley & Sons.

Sklar, B. & Kumar, P. (2017). *Digital Communications: Fundamentals and Applications* (ed. Second). Pearson.

Stüber, G. L. (2011). *Principles of mobile communication* (ed. 3rd ed). New York: Springer.

Talwar, S. & Paulraj, A. (1997). Blind separation of synchronous co-channel digital signals using an antenna array. II. Performance analysis. *IEEE Transactions on Signal Processing*, 45(3), 706–718. doi: 10.1109/78.558489.

Tepedelenlioglu, C., Rajan, A. & Zhang, Y. (2011). Applications of Stochastic Ordering to Wireless Communications. *IEEE Transactions on Wireless Communications*, 10(12), 4249–4257. doi: 10.1109/TWC.2011.093011.110187.

Tse, D. & Viswanath, P. (2006). *Fundamentals of wireless communication*. New York: Cambridge University Press.

Varanasi, M. K. (1995). Group detection for synchronous Gaussian code-division multiple-access channels. *IEEE Transactions on Information Theory*, 41(4), 1083–1096. doi: 10.1109/18.391251.

Yang, Y., Hu, J. & Zhang, H. (2007). Iterative Group MAP Detection in MIMO Wireless Systems. *2007 IEEE 66th Vehicular Technology Conference*, pp. 680–684. doi: 10.1109/VETECF.2007.152.

Yeo, K. S. (2023). *From 5G to 6G and Beyond*. WORLD SCIENTIFIC. doi: 10.1142/13265.

Zhang, Z., Wang, X., Long, K., Vasilakos, A. V. & Hanzo, L. (2015). Large-scale MIMO-based wireless backhaul in 5G networks. *IEEE Wireless Communications*, 22(5), 58–66. doi: 10.1109/MWC.2015.7306538.

Zhao, L., Zhao, H., Zheng, K. & Xiang, W. (2018). *Massive MIMO in 5G Networks: Selected Applications*. Cham: Springer International Publishing. doi: 10.1007/978-3-319-68409-3.

Zhu, X. & Murch, R. D. (2002). Performance analysis of maximum likelihood detection in a MIMO antenna system. *IEEE Transactions on Communications*, 50(2), 187–191. doi: 10.1109/26.983313.